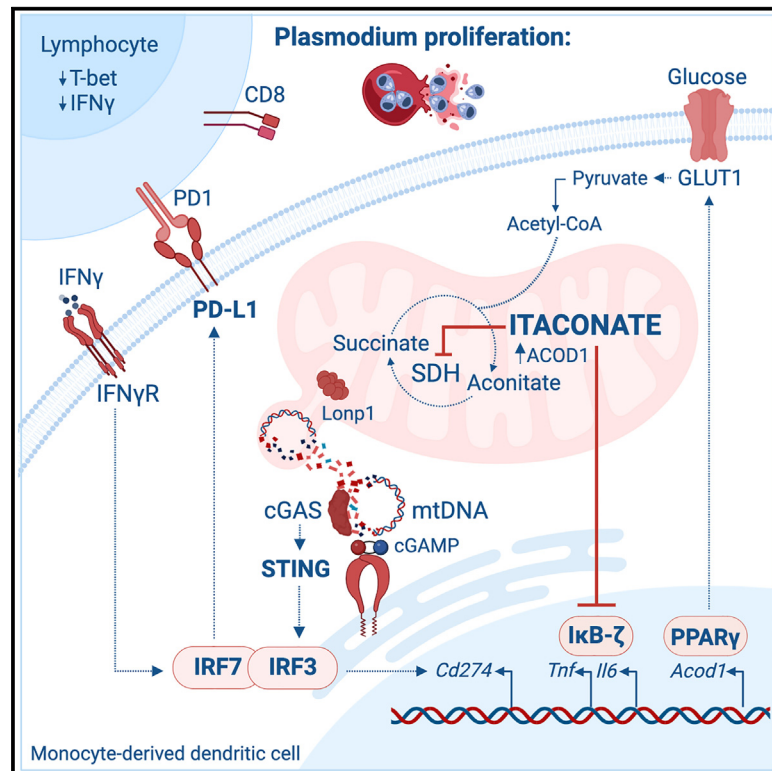


Cell Metabolism

Itaconate impairs immune control of *Plasmodium* by enhancing mtDNA-mediated PD-L1 expression in monocyte-derived dendritic cells

Graphical abstract



Authors

Theresa Ramalho, Patricia A. Assis, Ogooluwa Ojelabi, ..., Cole Haynes, Douglas T. Golenbock, Ricardo T. Gazzinelli

Correspondence

theresa.ramalho@umassmed.edu (T.R.), ricardo.gazzinelli@umassmed.edu (R.T.G.)

In brief

Ramalho et al. unveil that splenic monocyte-derived dendritic cells (MODCs) accumulate TCA cycle-derived itaconate in experimental malaria. Itaconate-induced mitochondrial disruption releases nucleic acids, which activate STING-IRF3/IRF7-mediated expression of PD-L1. In such a state, MODCs expressing PD-L1 impair immune-mediated control of *Plasmodium* by limiting the activation of CD8+ lymphocytes.

Highlights

- *Pc*-induced IFN γ boosts glycolysis in MODCs and itaconate accumulation *in vivo*
- Itaconate disrupts mitochondria, leading to nucleic acid release and MODC restraint
- mtDNA-mediated STING-IRF3/IRF7 pathway induces PD-L1 expression in MODCs
- PD-L1 expression by MODCs impairs CD8+ T cell activation and control of parasitemia



Article

Itaconate impairs immune control of *Plasmodium* by enhancing mtDNA-mediated PD-L1 expression in monocyte-derived dendritic cells

Theresa Ramalho,^{1,2,*} Patricia A. Assis,¹ Ogooluwa Ojelabi,¹ Lin Tan,³ Brener Carvalho,⁴ Luiz Gardinassi,⁵ Osvaldo Campos,⁶ Philip L. Lorenzi,³ Katherine A. Fitzgerald,¹ Cole Haynes,² Douglas T. Golenbock,¹ and Ricardo T. Gazzinelli^{1,4,7,8,*}

¹Department of Medicine, University of Massachusetts Chan Medical School, Worcester, MA, USA

²Department of Molecular Cell and Cancer Biology, University of Massachusetts Chan Medical School, Worcester, MA, USA

³Department of Bioinformatics and Computational Biology, University of Texas MD Cancer Center, Houston, TX, USA

⁴Instituto René Rachou, Fundação Oswaldo Cruz, Belo Horizonte, Minas Gerais, Brazil

⁵Instituto de Patologia Tropical e Saúde Pública, Universidade Federal de Goiás, Goiânia, Brazil

⁶Plataforma de Medicina Translacional, Fundação Oswaldo Cruz/Faculdade de Medicina de Ribeirão Preto, Ribeirão Preto, São Paulo, Brazil

⁷Centro de Tecnologia de Vacinas, Universidade Federal de Minas Gerais, Belo Horizonte, Minas Gerais, Brazil

⁸Lead contact

*Correspondence: theresa.ramalho@umassmed.edu (T.R.), ricardo.gazzinelli@umassmed.edu (R.T.G.)

<https://doi.org/10.1016/j.cmet.2024.01.008>

SUMMARY

Severe forms of malaria are associated with systemic inflammation and host metabolism disorders; however, the interplay between these outcomes is poorly understood. Using a *Plasmodium chabaudi* model of malaria, we demonstrate that interferon (IFN) γ boosts glycolysis in splenic monocyte-derived dendritic cells (MODCs), leading to itaconate accumulation and disruption in the TCA cycle. Increased itaconate levels reduce mitochondrial functionality, which associates with organellar nucleic acid release and MODC restraint. We hypothesize that dysfunctional mitochondria release degraded DNA into the cytosol. Once mitochondrial DNA is sensitized, the activation of IRF3 and IRF7 promotes the expression of IFN-stimulated genes and checkpoint markers. Indeed, depletion of the STING-IRF3/IRF7 axis reduces PD-L1 expression, enabling activation of CD8⁺ T cells that control parasite proliferation. In summary, mitochondrial disruption caused by itaconate in MODCs leads to a suppressive effect in CD8⁺ T cells, which enhances parasitemia. We provide evidence that ACOD1 and itaconate are potential targets for adjunct antimalarial therapy.

INTRODUCTION

Every year, approximately 200 million people are infected by *Plasmodium*, and around 400,000 children die of infection, contributing to social and economic instability in the developing world.¹ Malaria is a complex multisystemic disorder in which multiple parasite and host factors contribute to disease severity.² Many studies have documented the role of pro-inflammatory cytokines in malaria pathogenesis.² In addition, host metabolic changes, such as hypoglycemia and lactate accumulation (lactic acidosis), are often associated with severe forms of disease.³ Thus, understanding the metabolic mechanisms that mediate host resistance or susceptibility to infection is critical to improving the clinical management of individuals with malaria.

In the last few years, major advances have been made in associating the metabolic stage of immune cells and their function. Metabolites derived from the tricarboxylic acid (TCA) cycle synthesized in myeloid cells have immune-modulatory properties.⁴ The TCA cycle consists of a series of mitochondrial enzymatic

reactions in aerobic organisms to generate ATP via oxidation of acetyl-coenzyme A (CoA) derived from glucose/pyruvate, fatty acid oxidation, and anaplerosis from amino acids.⁵ In eukaryotes, the intermediates of the TCA cycle are retained in mitochondria. During cell stress, the mitochondrial membranes are destabilized, allowing the release of TCA cycle metabolites and danger signals into the cytosol, extracellular matrix, and/or plasma.⁶ When released, metabolites such as succinate, citrate, fumarate, and itaconate activate antioxidant pathways and exert post-translational modifications, which balances activation of immune cells.⁷

Recent studies demonstrated that alterations in host carbohydrate, lipid, protein, and heme metabolism are features of host susceptibility to *P. vivax* and *P. falciparum*. In the context of hypoglycemia, glucose intake in monocytes impairs mitochondrial functionality and reactive oxygen species production during the proliferative phase of *P. vivax*.⁸ Yet, systemic glutaminolysis is closely associated with impaired humoral immunity and exacerbated systemic inflammation in severe cases and models of



malaria.^{9,10} Similarly, evidence of lipid catabolism is often observed in individuals acutely infected with *P. falciparum* or *P. vivax*.^{11–13} Regardless of the original carbon source, the cellular metabolism of the malaria host contributes to an immunological state that favors *Plasmodium* proliferation.^{14,15} It determining which products generated from cellular metabolism in the hypoglycemic host support susceptibility, and understanding this process is critical to understanding malaria pathogenesis and developing prevention and treatment strategies.

By employing a metabolic compartmentalization approach, we observed enhanced glycolysis and accumulation of the TCA-cycle derivative itaconate in splenic monocyte-derived dendritic cells (MODCs) from *Plasmodium chabaudi* (*Pc*)-infected mice. During *Pc* infection, endogenous itaconate limits the release of pro-inflammatory cytokines by MODCs and shrinks lymphocyte activation, impairing parasite clearance. We hypothesize that mitochondrial dysfunction caused by itaconate in MODCs releases degraded mitochondrial DNA (mtDNA) and possibly double-stranded RNA (mtDNA). Once in cytosol, mtDNA activates cytosolic nucleic acid sensors and downstream transcription factors interferon regulatory factor (IRF)3 and IRF7. In addition to induction of interferon-stimulated genes (ISGs) in MODCs, IRF3 and IRF7 induce programmed cell death 1 ligand 1 (PD-L1, also known as CD274) expression in our model, which limits CD8+ T cell activation and impairs parasite clearance. Thus, in this mouse model of malaria, itaconate accumulation subverts MODC metabolism, which confers advantageous escape of *Pc* from host immunity.

RESULTS

Enhanced glycolysis in differentiated MODCs from *Pc*-infected mice

Studies performed in our laboratory demonstrate that in mice acutely infected with *Pc*, interferon (IFN) γ drives the differentiation of MODCs that produce high levels of tumor necrosis factor (TNF). We found that TNF enhances glucose processing in the spleen and liver, which culminates in a hypoglycemic state, control of parasite replication, and increased disease severity.¹⁶ Herein, we characterized the metabolism of differentiated MODCs during *Pc* infection and asked how their metabolic state affects the pathophysiology of experimental malaria.

To determine the metabolic state of MODCs from *Pc*-infected mice, we performed *ex vivo* and *in vivo* experiments with spleens and splenic MODCs from wild-type (WT) C57BL/6 and LysM/CRE-IFN γ R knockout mice by employing flow cytometry, western blot, and Seahorse analysis (Figure 1A). We observed high glucose uptake by splenocytes from *Pc*-infected compared with non-infected WT mice (Figures 1B and S1A). Consistently, the population of CD11b+ splenocytes (MODCs predominantly) showed an increased extracellular acidification rate (ECAR) (Figure 1C), suggesting increased glycolysis. As previously described, we confirmed the role of IFN γ in mediating MODC differentiation during *Plasmodium* infection (Figures 1D and S1B–S1E).^{17,18} The absence of IFN γ R in myeloid cells resulted in decreased expression of major histocompatibility complex (MHC) II and DCSign (Figures 1D–1F, S1C, and S1D). Importantly, we observed an IFN γ -dependent increase of GLUT1 expression on MODCs from *Pc*-infected mice, both *in vivo*

(Figures 1G, 1H, and S1E) and *in vitro* (Figures 1I–1K and S1F). Together, our results indicate that once differentiated, MODCs require glucose as a substrate for their metabolism and that IFN γ directly impacts glucose metabolism.

Differentiated MODCs from *Pc*-infected mice accumulate itaconate, which branches the TCA cycle

We have previously shown that hypoglycemia is associated with an increased expression of genes related to the TCA cycle in the spleen and liver from *Pc*-infected mice.¹⁶ We hypothesized that the enhanced glycolysis increases the synthesis of TCAs in the mitochondria of splenic MODCs. To address this hypothesis, we sorted splenic MODCs from acutely infected mice and quantified untargeted metabolites through ultra-high-resolution mass spectrometry. In addition, we performed a transcriptomic analysis of spleens from infected mice and monocytes from patients with malaria (Figure 2A). Here, we report that the high expression of the TCA-cycle-related genes in the spleen of infected mice depends on IFN γ (Figures 2B and 2C; Tables S1). Among the genes, *Aconitate dehydrogenase* (*Acod1*), also known as *Immune-Responsive Gene 1* (*Irg1*), was the most induced gene (Figures 2B and S2B). *Acod1* encodes an enzyme that converts aconitate into itaconate. As expected, MODCs of infected mice showed increased levels of most of the TCAs derived from the TCA cycle (Figures 2D and 2E; Table S2). Among all the metabolites detected in our metabolome, the dicarboxylic acid itaconate was the most abundant (Figures 2D and 2E). Consistently, in a dataset of mice infected with *Pc*, the signature of itaconate was elevated during *Plasmodium* proliferation in the acute phase of infection (Figure 2F). As itaconate is a potent immunoregulator,¹⁹ we speculated that it may undermine innate and acquired immunity during malaria.

Itaconate inhibits the activity of succinate dehydrogenase (SDH),²⁰ an enzyme that converts succinate to fumarate. We found that the expression of *Acod1*, but not *Sdh*, was enhanced in MODCs from infected mice (Figures S2C and S2D). As a consequence, the synthesis of fumarate in MODCs is limited, as shown by the high itaconate/fumarate ratio (Figure 2G). These findings were validated in monocytes from patients with malaria compared with non-infected individuals. The expression of genes related to mitochondrial metabolism is increased in peripheral monocytes from patients infected with *P. vivax* (Figure 2H; Table S3). Among those genes, *Acod1* showed the highest expression. Furthermore, while evaluating human datasets, the itaconate signature was also found in the plasma of patients infected with *P. vivax* (Figure 2I). In addition, *ACOD1* expression is upregulated when human monocytes are exposed to *P. falciparum*-infected red blood cells (iRBCs) *in vitro* (Figure 2J). Considering that itaconate disrupts the TCA cycle while reducing SDH activity, we next evaluated mitochondrial functionality in differentiated MODCs from *Pc*-infected mice.

The branched TCA cycle in MODCs from *Pc*-infected mice is associated with mitochondrial disruption

On one hand, the accumulation of TCA cycle metabolites may be an important determinant of the new transcriptional program of differentiated MODCs. On the other hand, the inherited

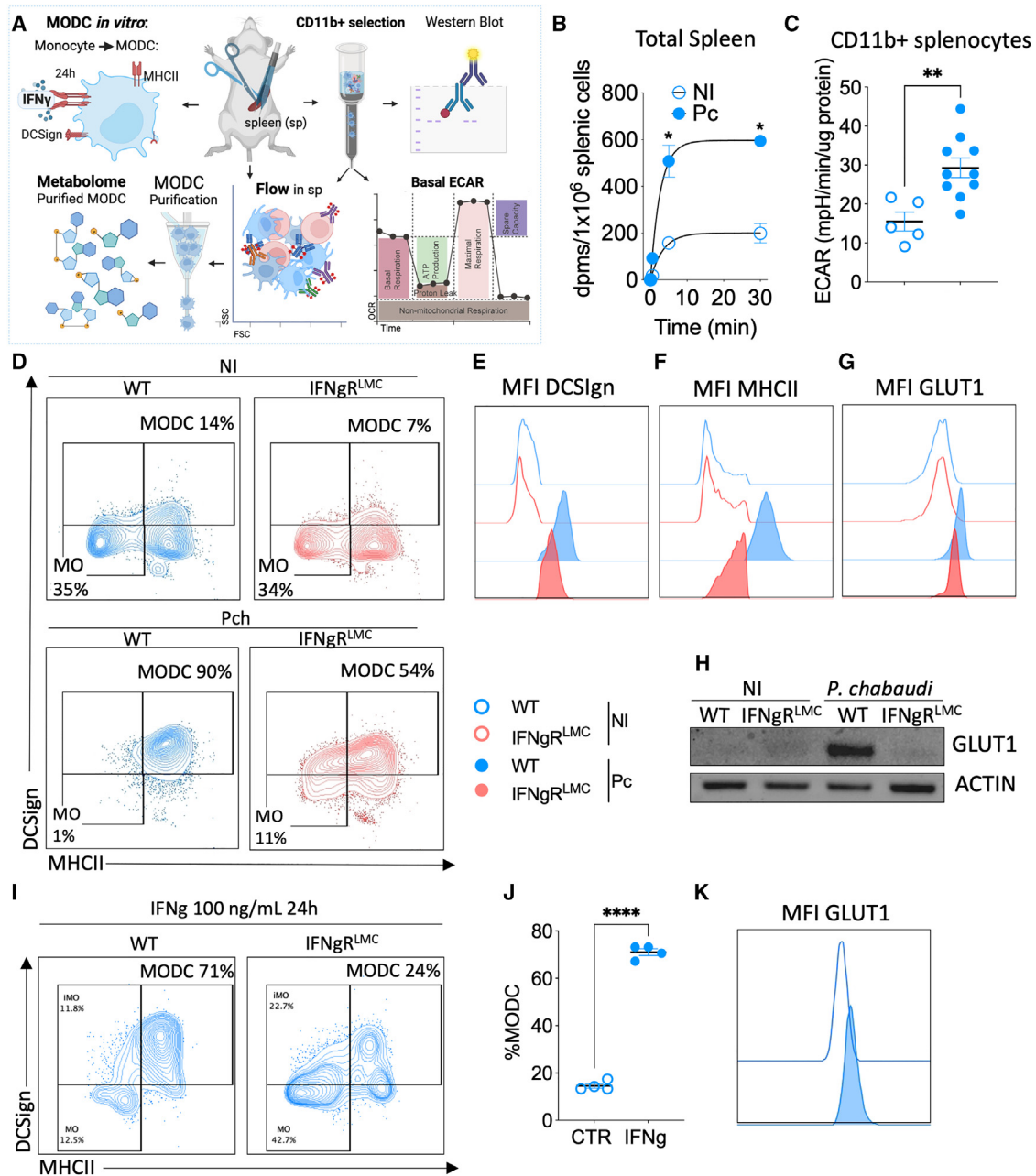


Figure 1. IFN γ enhances glucose metabolism during differentiation of monocyte-derived dendritic cells in *Pc*-infected mice

Schematic of techniques used to assess MODCs in the mouse spleen; created with BioRender.com (A). Glucose uptake with 2DG radioisotope in total splenocytes of *Pc*-infected and non-infected (NI) mice (B); data are from three experiments with a pool of 3 animals per group in each experiment. Extracellular acidification rate (ECAR) in CD11b⁺ splenocytes from *Pc*-infected mice compared with NI mice *ex vivo* (C); data are from a pool of two experiments with n = 5 NI mice and n = 10 infected mice. Detection of MODC frequency (D), Median fluorescence intensity (MFI) of dendritic cell (DC) markers DCSign (E), MHCII (F), and GLUT1 (G) expression in total spleen of WT or IFN γ ^{LysMCre} mice, *Pc*-infected or NI; data are from a pool of two experiments with n = 3 NI mice and n = 5 infected mice. GLUT1 expression in CD11b⁺ splenocytes from *Pc*-infected and NI mice (H); the uncropped image is in [Data S1](#). Detection of DC markers DCSign and MHCII (I) for determination of MODC frequency (J), and GLUT1 MFI (K) under IFN γ stimuli; data are from a pool of two experiments with n = 4 uninfected mice. All experiments were repeated 2 or 3 times yielding similar results. *p < 0.001–0.05 by Student's t test performed between two groups; one-way ANOVA followed by Tukey's post hoc test was performed among three or more groups.

mitochondria from monocytes may be insufficient for the high energetic demands of newly differentiated MODCs.

Our non-targeted lipidome shows that MODCs from *Pc*-infected mice have lower levels of triglycerides (Figure 3A;

Table S5), which indicates lipid utilization by mitochondria in MODCs. Also, MODCs increase the levels of different classes of membrane phospholipids, which is commonly observed in newly differentiated cells (Figure 3A; Table S4). Among the

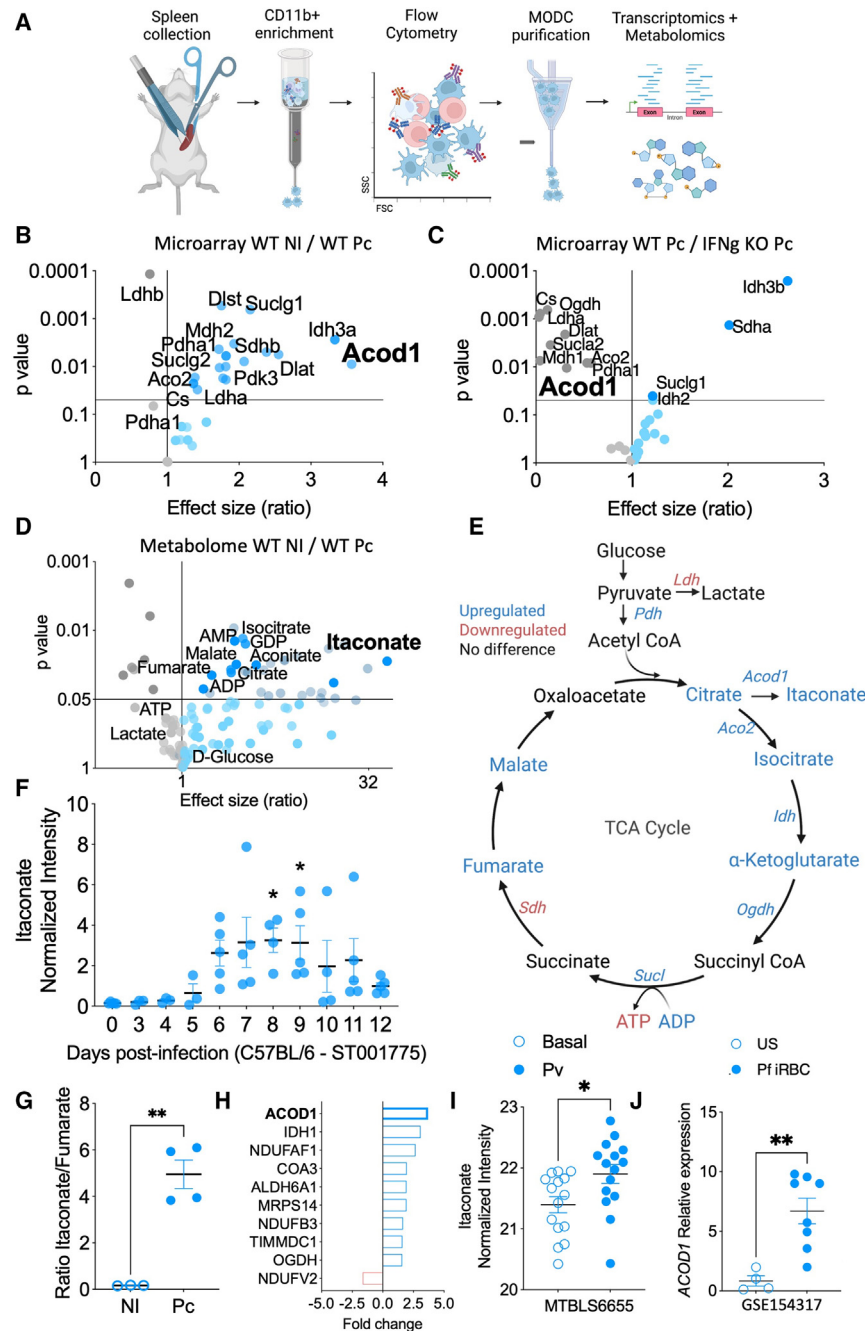


Figure 2. Glucose oxidation disrupts the TCA cycle in monocyte-derived dendritic cells of *Pc*-infected mice

Schematic of techniques used to assess metabolites and transcripts in MODCs from infected mice; illustration created with BioRender.com (A). Fold change of differentially expressed genes (DEGs) in *Pc*-infected WT mice relative to non-infected (NI) WT mice (B), and fold change of DEGs in *Pc*-infected IFN γ ^{-/-} mice relative to *Pc*-infected WT mice (C); data are from two experiments pooled with n = 3 mice in each group. Volcano plot showing the fold change and p values in metabolite intensity values of *Pc*-infected WT mice relative to NI WT mice; data are from two experiments pooled with n = 3 samples in NI mice, and n = 4 samples in the infected group, with 5 mice pooled per sample (access <https://doi.org/10.5281/zenodo.7608255>) (D). A cross-analysis of the metabolome and transcriptome established the metabolic phenotype of MODCs (E). Itaconate levels in the plasma of *Pc*-infected mice; two experiments pooled with n = 5 mice in the infected group (access <https://doi.org/10.21228/M8RX1D>) (F). The ratio of itaconate/fumarate was calculated from intensity values of each metabolite in the metabolome of *Pc*-infected or NI mice (G); data are from two experiments pooled with n = 3 samples from the NI group and n = 4 samples from the infected group, with 5 mice pooled per sample. Experiments in (B)–(D), (F), and (G) were repeated 2 or 3 times yielding similar results. RNA sequencing (RNA-seq) performed in monocytes from NI individuals (n = 5) or individuals infected with *P. vivax* (n = 5). Fold change in gene expression of *P. vivax*-infected relative to NI individuals (access <https://doi.org/10.5281/zenodo.7683360>) (H). Identification of the itaconate signature in the plasma from *P. vivax*-infected individuals (MetaboLights: MTBLS665) (I) n = 15 in each experimental group, or *ACOD1* expression in monocytes stimulated or not with *P. falciparum*-infected erythrocytes; data are from n = 4 samples in non-stimulated monocytes and n = 8 samples in monocytes stimulated with iRBCs (GEO: GSE154317) (J). * p < 0.001–0.05 by Student’s t test performed between two groups.

phospholipids, the accumulation of ceramides and phosphatidylserines indicates cell stress and programmed cell death in MODCs^{21,22} and the accumulation of phosphatidylethanolamine and cardiolipins strongly suggests alterations in mitochondrial structure (Figure 3A; Table S4). The composition of cardiolipins found in our metabolome shows elongation and additional saturated bonds—which are both signs of modulation of the electron transport chain (ETC)²³ (Figure 3A; Table S4). Indeed, we observed that MODCs accumulate more ADP than ATP (Figures 3B and 3C), indicating a disturbance in the ETC and ATP synthesis. Furthermore, MODCs express low protein levels

of the complex II subunit SDHB (Figure 3D), corroborating the hypothesis of immature ETC machinery in differentiated MODCs. Consistently, MODCs from infected (or IFN γ -induced) mice have a lower frequency of functional mitochondria compared with monocytes (Figure 3E). When we enforce mitochondrial activity with galactose-derived substrates, the frequency of functional mitochondria is even more reduced (Figures S3A–S3C). This functional assay indicates that substrates utilized by mitochondrial respiration contribute to mitochondrial dysfunction, which reflects compromised ATP synthesis and structural changes in mitochondria. Together, these results show that differentiated MODCs are in a metabolic state that accumulates intermediates of the TCA cycle and disrupts mitochondrial functionality.

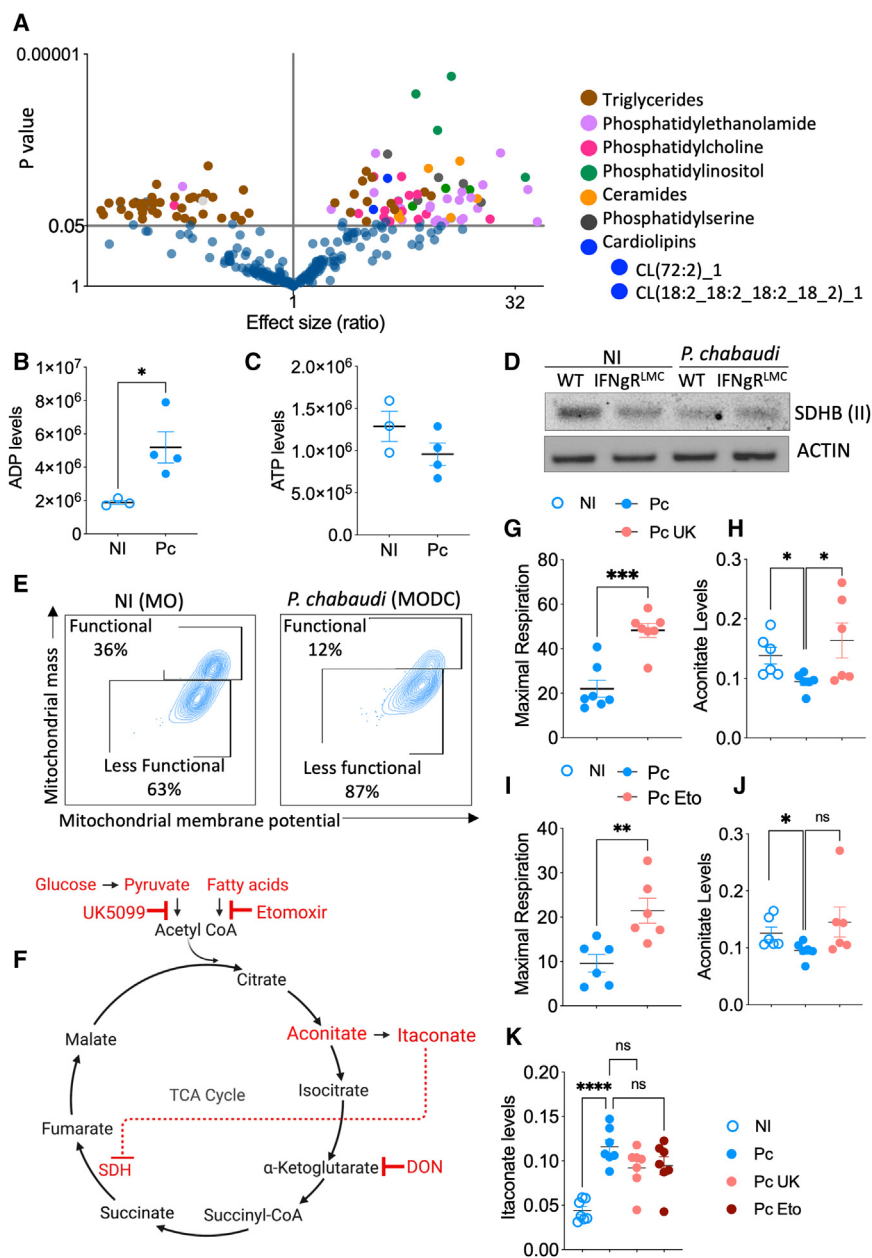


Figure 3. Mitochondria functionality is compromised in monocyte-derived dendritic cells from *Pc*-infected mice

Volcano plot of the fold change and p values of lipid intensity values of *Pc*-infected (*Pc*) WT mice relative to non-infected (NI) WT mice (access <https://doi.org/10.5281/zenodo.7608255>) (A). Intensity values of ADP (B) and ATP (C) in the metabolome of MODCs from infected or NI WT mice. Results from the lipidome and metabolome were pooled from two experiments with $n = 3$ samples in the NI group and $n = 4$ samples in the infected group, with five mice pooled per sample. SDHB expression in CD11b+ splenocytes selected from *Pc*-infected or NI mice; uncropped images are in [Data S1](#) (D). Mitochondrial functionality in MODCs of *Pc*-infected or MO (monocytes) in NI mice (E). Scheme demonstrating the targets of the drugs utilized to treat CD11b+ splenocytes from infected mice (F). Maximal respiration (G) and aconitate levels (H) in CD11b+ splenocytes isolated from *Pc*-infected mice treated with UK5099 or DMSO from two experiments pooled with $n = 7$ mice per group. Maximal respiration and aconitate levels in CD11b+ splenocytes isolated from *Pc*-infected mice treated with etomoxir (I) or DMSO (J) from two experiments pooled with $n = 6$ mice per group. Itaconate levels in the supernatant of CD11b+ splenocytes treated with UK5099 or etomoxir from two experiments pooled with $n = 7$ mice per group (K). * $p < 0.001$ – 0.05 by Student's *t* test performed between two groups. Experiments were repeated 2 or 3 times yielding similar results.

Compromised mitochondrial functionality results in impaired oxygen consumption by the cell. Because substrates used by mitochondrial respiration contribute to the loss of mitochondrial functionality in MODCs, we next evaluated which substrates impair respiration and the TCA cycle in these cells (Figure 3F). Indeed, we observed that MODCs from infected mice have impaired oxygen consumption (Figure S3D). When pyruvate availability to mitochondria was limited using UK5099, maximal oxygen consumption was improved (Figures 3G and S3E), and aconitate levels were restored (Figure 3H). Aconitate is an intermediate metabolite synthesized from citrate that is the substrate for itaconate synthesis. Hence, when itaconate is synthesized, aconitate levels are reduced. Importantly, we observed that etomoxir, an inhibitor of fatty acid oxidation also improves mitochondrial maximal capacity and partially recovers aconitate levels (Figures 3I, 3J, and S3F),

while anaplerosis from glutamate did not reverse the disturbance in oxygen consumption by MODCs (Figure S3G). We observed a discrete reduction in itaconate levels when cells were treated with either UK5099 or Eto (Figure 3K). Either treatment restored aconitate levels, indicating that both metabolic pathways are needed to convert aconitate from citrate and decrease itaconate accumulation. Altogether, these results indicate that pyruvate generated from glucose or fatty acids, but not amino acids, enhanced the TCA cycle activity and contributed to itaconate accumulation and mitochondrial maladaptation in MODCs from *Pc*-infected mice. We next explored how the activation of a transcription factor that classically induces lipid and glucose metabolism sustains the metabolic status found in MODCs of *Plasmodium*-infected mice.

PPAR γ activation sustains MODC differentiation and its metabolic state in *Plasmodium*-infected mice

We previously determined that the expression of peroxisome proliferator-activated receptor gamma (PPAR γ) follows glucose and parasite synchronization both in the liver and spleen from *Pc*-infected mice, suggesting the potential role of PPAR γ as a mediator of glucose metabolism in host cells.¹⁶ PPAR γ is a nuclear receptor

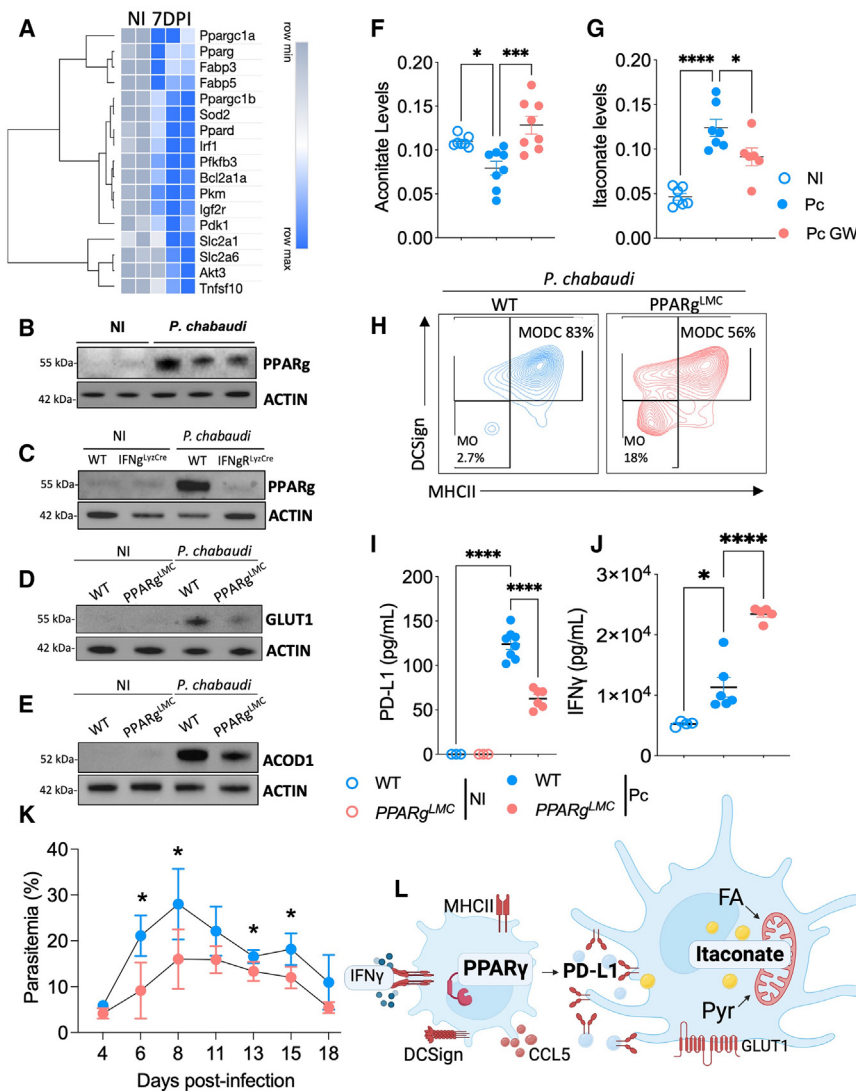


Figure 4. PPAR γ activation sustains the differentiation and metabolic state of monocyte-derived dendritic cells

Heatmap showing the relative expression of markers of the PPAR γ pathway in MODCs from *Plasmodium berghei Anka (PbA)*-infected or non-infected (NI) mice (GEO: GSE126381) (A); results shown were pooled from two experiments with $n = 2$ NI mice and $n = 3$ infected mice. Western blots to analyze PPAR γ in CD11b⁺ splenocytes from WT or IFN γ R^{LysMCre} mice that were *Pc*-infected or NI (B and C). GLUT1 (D) and ACOD1 (E) expression in CD11b⁺ splenocytes from NI or *Pc*-infected WT or PPAR γ ^{LysMCre} mice; uncropped images are in Data S1. Aconitate (F) and itaconate (G) levels in CD11b⁺ splenocytes from *Pc*-infected mice treated *ex vivo* with GW9662; data are from two experiments pooled with $n = 7$ mice per group. Frequency of MODCs in CD11b⁺ splenocytes from NI or *Pc*-infected WT or PPAR γ ^{LysMCre} mice (H); data are from two experiments pooled with $n = 8$ mice in each group. Expression of PD-L1 in MODCs (I) from two experiments pooled with $n = 3$ NI mice and $n = 6$ infected mice, and systemic levels of IFN γ in WT or PPAR γ ^{LysMCre} mice that were NI or *Pc*-infected (J); data are from two experiments pooled with $n = 4$ mice per group. Parasitemia in WT or PPAR γ ^{LysMCre} mice (K) from two experiments pooled with $n = 6$ mice per group. Model showing IFN γ -induced differentiation of MODCs *in vivo* and *in vitro* leads to enhanced PPAR γ expression and function, promoting itaconate synthesis that culminates in the expression of GLUT1 and PD-L1 by MODCs from *Pc*-infected mice; illustration created with BioRender.com (L). Experiments were repeated 2 or 3 times yielding similar results. * $p < 0.001$ – 0.05 by Student's *t* test performed between two groups. One-way ANOVA followed by Tukey's post hoc test was performed among three or more groups.

commonly activated in different subsets of differentiated DCs. PPAR γ is known to promote glucose uptake by different cell types. For this reason, it is a molecular target of thiazolidinediones that are used to normalize the levels of circulating glucose in individuals with diabetes.²⁴ In addition to inducing glucose uptake, PPAR γ induces oxidation of fatty acids and mitochondrial biogenesis. Thus, the PPAR γ pathway may be an important factor for itaconate accumulation in MODCs from *Pc*-infected mice.

Various genes involved in the PPAR γ pathway are upregulated in MODCs from *Plasmodium*-infected mice (Figure 4A; Table S5). Most of these PPAR γ -related genes are involved in fatty acid and glucose metabolism (Table S5). An activated PPAR γ transcriptional signature was also observed in monocytes from individuals with *P. falciparum* malaria, and in monocytes stimulated with infected RBCs (Figures S4A and S4B). Importantly, we determined that IFN γ signaling induced the expression of PPAR γ protein in MODCs (Figures 4B and 4C). Yet, protein expression of GLUT1 (Figure 4D) and ACOD1 (Figure 4E) are increased downstream of PPAR γ activation. Accordingly, GLUT1 expression is not increased, and mitochondrial functionality is recovered in

MODCs when splenocytes are incubated *ex vivo* with GW9662, an irreversible antagonist of PPAR γ (Figures S4C and S4D). While GW9662 treatment also improves maximal oxygen consumption in MODCs of infected mice (Figure S4E). These results are consistent with the hypothesis that once PPAR γ is activated during MODC differentiation by IFN γ stimuli, increased glucose uptake increases substrate availability for itaconate synthesis. Indeed, *ex vivo* PPAR γ inhibition recovers aconitate levels (Figure 4F), while reducing itaconate levels (Figure 4G).

We also found that PPAR γ mediates the increase of MHCII expression, and, thus, the differentiation of MODCs (Figures 4H and S4F–S4H), which is consistent with the decreased secretion of CCL5 when CD11b⁺ splenocytes from *Pc*-infected mice are treated *ex vivo* with GW9662 (Figure S4I). Due to PPAR γ effects on MODC maturation and previously reported effects of itaconate on macrophage activation, we evaluated whether PD-L1 expression was enhanced on MODCs. PD-L1 is a co-inhibitory ligand often expressed by activated antigen-presenting cells. When expressed, PD-L1 promotes exhaustion in CD8⁺ T cell activation.²⁵ We found less PD-L1 secreted by MODCs from *Pc*-infected

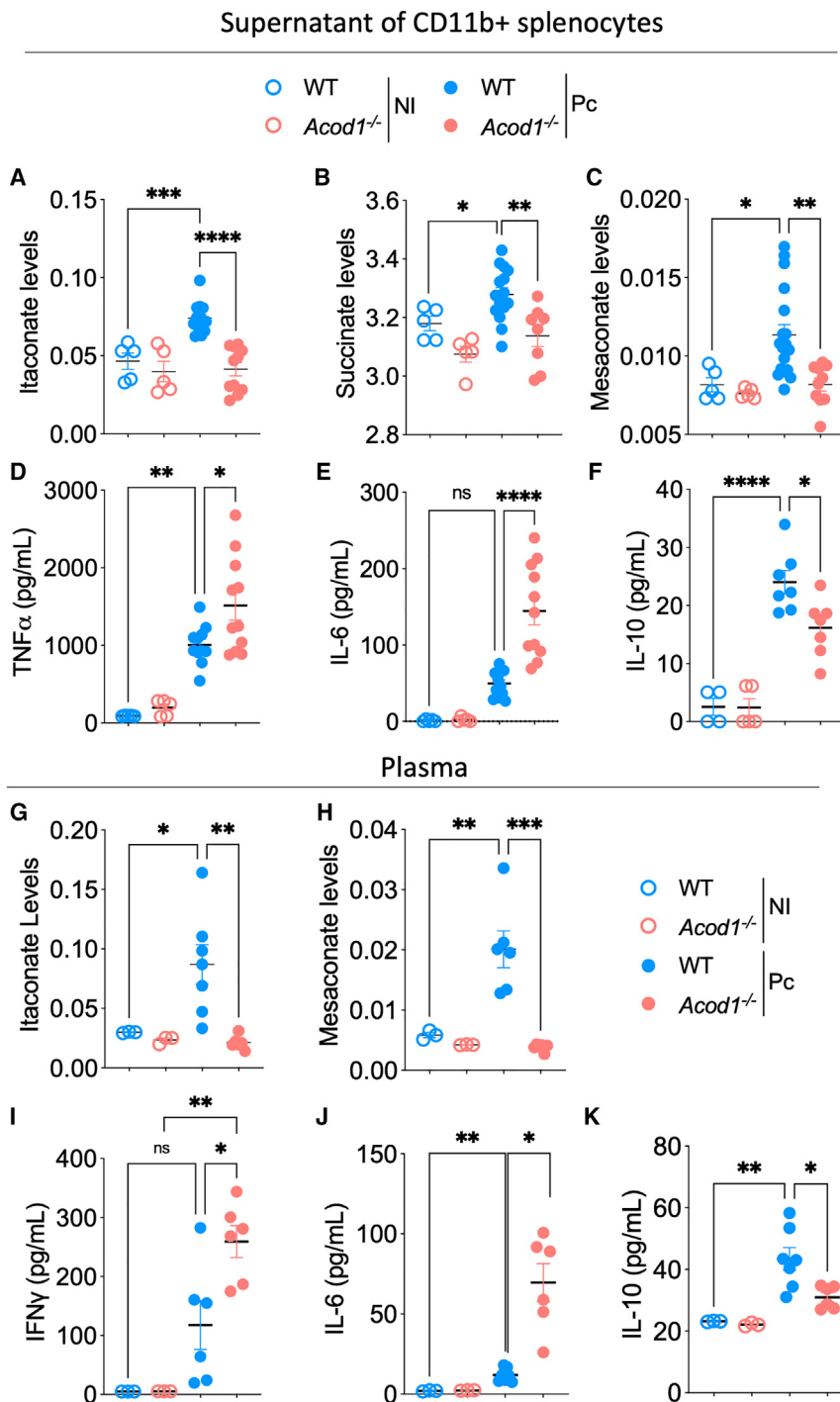


Figure 5. Endogenous itaconate regulates immune responses in *Pc*-infected mice

CD11b+ splenocytes from WT or *Acod1*^{-/-} mice that were *Pc*-infected or non-infected (NI), were incubated *ex vivo*, and the supernatant harvested after 4 h. The changes in itaconate (A), succinate (B), and mesaconate (C) levels were assessed by ultra-high resolution mass spectrometry from two experiments pooled with n = 5 NI mice and n = 10 infected mice. The levels of TNF α (D), IL-6 (E), and IL-10 (F) were measured by cytometric bead array from two experiments pooled with n = 5 NI mice and n = 10 infected mice. In the plasma of WT or *Acod1*^{-/-} mice that were *Pc*-infected or NI, itaconate (G) and mesaconate (H) levels were assessed by mass spectrometry from two experiments pooled with n = 3 for the NI group and n = 6 for the infected group. The IFN γ (I), IL-6 (J), and IL-10 (K) levels were quantified by cytometric bead array from two experiments pooled with n = 3 for the NI group and n = 6 for the infected group. Experiments were repeated 2 or 3 times yielding similar results. *p < 0.001–0.05 by Student's t test performed between two groups. One-way ANOVA followed by Tukey's post hoc test was performed among three or more groups.

Itaconate derived from MODCs regulates systemic inflammation in *Plasmodium* infection

Itaconate is an immune regulator induced in myeloid cells in conditions of experimental systemic inflammation, such as tuberculosis, sepsis, psoriasis, myocarditis, and gout.¹⁹ Similarly, PPAR γ is considered an immune regulator because it limits the activation of nuclear factor kappa B (NF- κ B) in macrophages.²⁶ In our model, PPAR γ activation contributes to MODC maturation and itaconate synthesis; thus, we hypothesized that itaconate could regulate the immune response in malaria by limiting MODC activation.

Our targeted metabolome showed that when MODCs from infected mice are incubated *in vitro* for 4 h, they release high levels of itaconate and succinate (Figures 5A and 5B). Interestingly, succinate release is ACOD1 dependent (Figure 5B), corroborating the hypothesis that itaconate reduces the processing of succinate into fumarate (Figure 2E), leading to succinate accumulation in the supernatant. Hence, we hypothesize that itaconate directly regulates the function of MODCs and, as a consequence, the immune response. We observed that MODCs of infected mice also release mesaconate into the supernatant (Figure 5C). Mesaconate is an immunoregulatory metabolite generated from itaconate conversion.^{27,28} Importantly, in an itaconate-free system, MODCs from infected mice secrete more TNF and interleukin (IL)-6 (Figures 5D and 5E), while IL-10 secretion is reduced (Figure 5F).

LysM-PPAR γ ^{-/-} mice compared with WT (Figure 4I). Not surprisingly, IFN γ levels are elevated in the plasma of LysM-PPAR γ ^{-/-} mice compared with WT mice infected with *Pc* (Figure 4J). Consistently, LysM-PPAR γ ^{-/-} mice have better control of *Plasmodium* proliferation (Figure 4K). Altogether, these results suggest that PPAR γ activation in differentiated MODCs contributes to a metabolic state that leads to the accumulation of the TCA-cycle-derived itaconate. In this scenario, PPAR γ -mediated PD-L1 seems to limit the activation of lymphocytes systemically (Figure 4L).

nate into fumarate (Figure 2E), leading to succinate accumulation in the supernatant. Hence, we hypothesize that itaconate directly regulates the function of MODCs and, as a consequence, the immune response. We observed that MODCs of infected mice also release mesaconate into the supernatant (Figure 5C). Mesaconate is an immunoregulatory metabolite generated from itaconate conversion.^{27,28} Importantly, in an itaconate-free system, MODCs from infected mice secrete more TNF and interleukin (IL)-6 (Figures 5D and 5E), while IL-10 secretion is reduced (Figure 5F).

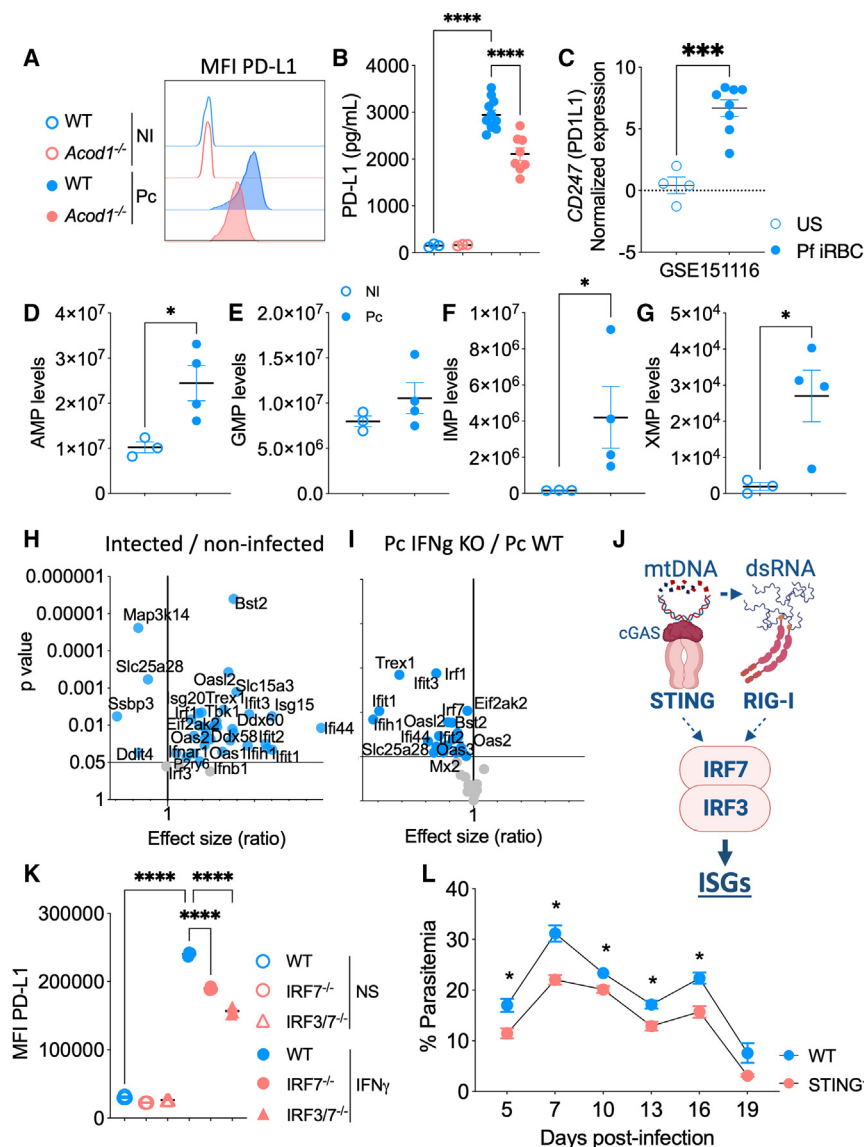


Figure 6. PD-L1 expression on MODCs is induced by STING-IRF3/IRF7

Expression of PD-L1 by MODCs of *Pc*-infected and non-infected (NI) WT or *Acod1*^{-/-} mice (A). Quantification of PD-L1 in the plasma of *Pc*-infected or non-infected (NI) WT or *Acod1*^{-/-} mice from two experiments pooled with n = 3 in the NI group and n = 6 in the infected group (B). Human monocytes stimulated with *Pf*-iRBCs (C); data are from n = 4 unstimulated samples and n = 8 *Pf*-stimulated samples. Levels of AMP (D), GMP (E), IMP (F), and XMP (G) in the metabolome of MODCs from *Pc*-infected and NI mice from two experiments pooled with n = 3 samples in the NI group and n = 4 samples in the infected group, with 5 mice pooled per sample. Volcano plot showing the fold change and p values in gene expression values of *Pc*-infected relative to NI WT mice (H), and fold change and p values in gene expression values of *Pc*-infected IFN γ ^{-/-} relative to *Pc*-infected WT mice (I); data are from two experiments pooled with n = 3 in each group. Schematic showing IRF3 and IRF7 activation by STING and RIG-I; created with BioRender.com (J). Expression of PD-L1 in non-stimulated iBMDMs and in IFN γ -stimulated WT, IRF3^{-/-}, IRF7^{-/-}, and IRF3/IRF7 double knockout mice (K); data are from three experiments pooled with n = 3 per group. Parasitemia from WT and STING^{-/-} mice infected with *Pc* (L); data are from two experiments pooled with n = 6 per group. Experiments were repeated 2 or 3 times yielding similar results. *p < 0.001–0.05 by Student's t test performed between two groups. One-way ANOVA followed by Tukey's post hoc test was performed among three or more groups.

(Figures 6A and S5A). Consistently, the increased levels of PD-L1 in the plasma of *Pc*-infected mice relied on itaconate (Figure 6B). Not surprisingly, the expression of *CD274*, which transcribes PD-L1 in humans (PD1L1 protein), is increased when human monocytes are stimulated with *P. falciparum*-infected

RBCs (Figure 6C). Additionally, individuals acutely infected with *P. falciparum* have increased expression of *CD274* in monocytes, which is sustained in convalescent individuals (Figure S5B). We found no evidence that itaconate affects the expression of the co-stimulatory receptors CD80 or CD86 (Figures S5C and S5D). Recent *in vitro* studies have shown that exogenous itaconate exerts mechanistic anti-inflammatory effects by promoting nuclear factor erythroid 2-related factor 2 (NRF2) and/or activating transcription factor 3 (ATF3) pathways.²⁹ We did not observe increased expression of NRF2 in CD11b+ cells from *Pc*-infected WT mice. In addition, the itaconate derivative 4-octyl-itaconate (4-OI) was unable to induce NRF2 by CD11b+ cells from *Pc*-infected *Acod1*^{-/-} mice (Figure S5E). ATF3 deactivates I κ B ζ , which induces the transcription of IL-6 and TNF. I κ B ζ is downregulated in cells from *Pc*-infected WT mice, but not in the *Acod1*^{-/-} mice, suggesting that ATF3 is activated in MODCs from *Pc*-infected mice. Consistently, 4-OI treatment inhibited the expression of I κ B ζ in CD11b+ *Acod1*^{-/-} cells (Figure S5F). However, 4-OI did not

Endogenous itaconate induces the expression of PD-L1 in a STING-IRF3/IRF7-dependent pathway

Next, we evaluated the expression of co-inhibitory and co-stimulatory ligands on MODCs, which are important for (de)activation of lymphocytes. We observed that MODCs of *Acod1*^{-/-} mice have reduced expression of the co-inhibitory factor PD-L1

Furthermore, the levels of both itaconate and mesaconate are increased in the plasma of infected mice (Figures 5G and 5H). As the levels of itaconate are greater compared with mesaconate, we hypothesized that the partial conversion of itaconate into mesaconate in MODCs (Figure 5C) is reflected systemically in the peripheral plasma. Thus, the high itaconate/mesaconate ratio in the plasma also suggests that mesaconate can act as an adjuvant to the regulatory effects of itaconate. Consistently, in *Plasmodium*-infected *Acod1*^{-/-} mice, the levels of circulating IFN γ and IL-6 are increased (Figures 5I and 5J), whereas the IL-10 levels in plasma are lower (Figure 5K).

Furthermore, the levels of both itaconate and mesaconate are increased in the plasma of infected mice (Figures 5G and 5H). As the levels of itaconate are greater compared with mesaconate, we hypothesized that the partial conversion of itaconate into mesaconate in MODCs (Figure 5C) is reflected systemically in the peripheral plasma. Thus, the high itaconate/mesaconate ratio in the plasma also suggests that mesaconate can act as an adjuvant to the regulatory effects of itaconate. Consistently, in *Plasmodium*-infected *Acod1*^{-/-} mice, the levels of circulating IFN γ and IL-6 are increased (Figures 5I and 5J), whereas the IL-10 levels in plasma are lower (Figure 5K).

induce ATF3 expression in CD11b+ from *Acod1*^{-/-} cells of *Pc*-infected mice (Figure S5E). Hence, we suggest that the lower levels of TNF α and IL-6 secreted by CD11b+ from WT MODCs (Figures 5D and 5E), as compared with *Acod1*^{-/-} MODCs from *Pc*-infected mice, explain the negative effects of endogenous itaconate on I κ B ζ , although the ATF3 pathway was not enriched in our omics data analysis.

To further evaluate the autocrine effect of itaconate on PD-L1 expression, we decided to investigate if other signaling pathways that are concomitantly enriched in our omics analysis could integrate the itaconate/PD-L1 axis. In MODCs from *Pc*-infected WT mice, we found increased levels of products from cyclic nucleotide metabolism, such as adenosine monophosphate (AMP), guanosine monophosphate (GMP), inosine monophosphate (IMP), xanthosine monophosphate (XMP), adenosine diphosphate (ADP), and guanosine diphosphate (GDP) (Figures 6D–6G and S5G; Table S2), indicating that the metabolism of nucleoside tri- and diphosphates is enhanced. Furthermore, the transcriptome of MODCs from infected mice shows increased expression of transcripts that promote mtDNA degradation and leakage (Figure S5H). Yet, the lower expression of transcripts related to mtDNA synthesis was found in our analysis (Figure S5I).

Importantly, we found that retinoic acid-inducible gene I (RigI, also known as Ddx58), interferon-induced with helicase C domain 1 (Mda5, also known as Ifih1), TANK-binding kinase 1 (Tbk1), and the transcription factors IRF1, IRF3, and IRF7 are differentially expressed in splenocytes from *Pc*-infected WT mice, but not in the IFN γ ^{-/-} mice (Figures 6H and 6I; Table S1). We hypothesize that IFN γ induces the synthesis and accumulation of itaconate leading to a brake in the TCA cycle and accumulation of succinate. Mitochondria dysfunction potentially results in leakage of mtDNA and mtdsRNA into the MODC cytosol. We hypothesized that the cyclic GMP-AMP synthase (cGAS) senses fragments of the mitochondrial genome³⁰ and activates the stimulator of interferon response cGAMP interactor 1 (STING),³⁰ whereas RIG-I and MDA5 sense mtdsRNA and activate the mitochondrial antiviral signaling protein (MAVS).^{31,32} STING and MAVS activate TBK1 to induce IRF3 and IRF7 expression and upregulate the expression of PD-L1 (Figure 6J). Indeed, our results show that in IFN γ -primed immortalized bone marrow-derived macrophages (iBMDMs), STING1^{-/-}, IRF7^{-/-}, or IRF3/IRF7 double knockout cells express lower levels of PD-L1 compared with WT iBMDMs cultured in similar conditions (Figure 6K). Importantly, a study proposed that the overexpression of Lon, a multiple-function protein that has proteolytic, chaperone, and DNA-binding activities, promotes mtDNA leakage in tumor cells.³³ Interestingly, when we treated IFN γ -stimulated iBMDMs with 2-cyano-3,12-dioxooleana-1,9-dien-28-oic acid (CDDO), a specific Lon inhibitor, the expression of PD-L1 was downregulated (Figure S5J).

Therefore, in IFN γ -induced MODCs from *Pc*-infected mice, accumulation of itaconate results in a Lon-dependent leakage of mtDNA fragments to the cytosol, activating cGAS and STING and leading to enhanced PD-L1 expression mediated by IRF3 and IRF7. It is possible that mtdsRNA also plays a role in this process by activating RIG-I/MDA5, MAVS, and TBK1, as these factors are highly induced in MODCs from infected mice (Figures 6H and 6I; Table S5). Importantly, STING^{-/-} mice show an enhanced resistance to *Pc* infection (Figure 6L). As we identified a close correlation between increased expression

of *ACOD1* and regulatory genes in monocytes of *Plasmodium*-infected subjects, we suggest that the accumulation of itaconate on MODCs in our murine model corresponds to malaria susceptibility.

Endogenous itaconate limits the activated state of CD8+ T cells leading to *Pc* proliferation

Although the frequency of CD4+Tbet+ T lymphocytes was significantly increased in *Acod1*^{-/-} mice (Figure 7A), the absence of itaconate only marginally increased the expression of IFN γ and CXCR3 expression by CD4+ T cells (Figures 7B, 7C, and S6A–S6D). Yet, the activation of CD8+ T cells is clearly downregulated by itaconate, as we observed increased frequencies of CD8+Tbet+CXCR3+IFN γ + T cells in itaconate-free mice (Figures 7D–7F, S6A, and S6E–S6G). The limited activation of T cells is consistent with limited levels of IFN γ found in the plasma of *Pc*-infected WT mice (Figure 5I). We also found increased expression of programmed cell death protein 1 (PD1) encoded by the *PDCD1* gene in lymphocytes of individuals infected with *P. falciparum* (Figure 7G). Accordingly, the improved immune response in the absence of itaconate results in lower parasitemia in *Acod1*^{-/-} mice (Figure 7H). Lastly, to validate the relevance of CD8+ T cell activation in host resistance to *Plasmodium*, we depleted CD8+ T cells by treating *Pc*-infected *Acod1*^{-/-} mice with an anti-CD8 monoclonal antibody. Importantly, *Acod1*^{-/-} mice treated with anti-CD8 were no longer able to control parasitemia (Figure 7I). Altogether, our results indicate that itaconate synthesized by MODCs limits the activation of CD8+ T cell function through STING-IRF3/IRF7-induced PD-L1 expression, impairing immune control of parasitemia in the *Pc* malaria model.

DISCUSSION

Monocytes are highly plastic cells that differentiate and specialize in different functions such as tissue repair, sensing invasive microorganisms, and initiating protective immune responses. MODCs are specialized in antigen presentation and shaping T cell-mediated immunity but also release bulk amounts of pro-inflammatory cytokines and display phagocytic function to destroy pathogens. We have described in experimental malaria models that MODCs transiently become the main DC population in spleens and inflamed non-lymphoid tissues during acute disease. When differentiated, MODCs promote inflammation and tissue damage, in experimental models of cerebral malaria¹⁷ and acute respiratory distress syndrome.³⁴ In this study, we examined how energy metabolism affects the differentiation and activation of MODCs. We observed that, during an acute infection with *Plasmodium*, glycolysis is enhanced in MODCs. Importantly, glucose metabolism sustains a mitochondrial adaptation that triggers the accumulation of TCA-cycle-derived metabolites with immunoregulatory properties. From these metabolites, the dicarboxylic acid itaconate derived from aconitate is the most abundant in MODCs and plasma of infected mice. While limiting cytokine release, itaconate promotes PD-L1 expression by MODCs via the STING/IRF3/IRF7 pathway, making CD8+ T cells less responsive and enhancing host susceptibility to *Pc* infection.

In malaria, CD4+ T and CD8+ T lymphocytes, as well as natural killer (NK) cells, release IFN γ that primes monocytic cells. Upon

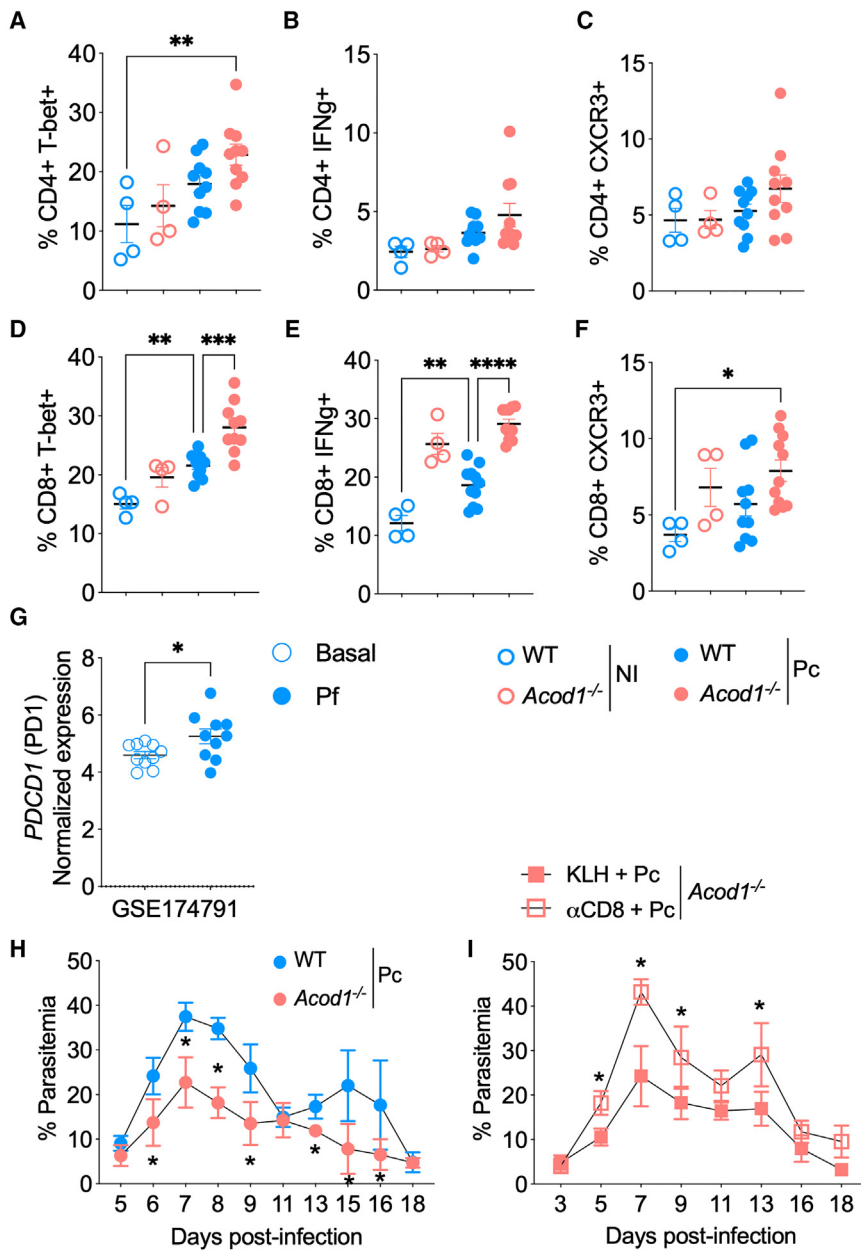


Figure 7. Endogenous itaconate limits the activation of CD8+ T cells and enhances susceptibility to *Pc* infection

Detection of T-bet (A), IFN γ (B), and CXCR3 (C) in splenic CD4+ T cells from WT or *Acod1*^{-/-} mice infected or not with (*Pc*). The expression of the same activation markers was also evaluated in CD8+ T cells (D–F); data are from two experiments pooled with n = 4 in the non-infected group and n = 10 in the infected group. Human dataset ID GEO: GSE174791 from the Gene Expression Omnibus was used to evaluate the expression of PDCD1 in T cells from *P. falciparum*-infected individuals (n = 10) compared with non-infected individuals (n = 10) (G). Parasitemia levels calculated from the blood smears of *Pc*-infected WT and *Acod1*^{-/-} mice (H). Parasitemia levels calculated from the blood smears of *Pc*-infected *Acod1*^{-/-} mice treated or not with anti- α -CD8 antibodies (I); data are from two experiments pooled with n = 6 infected mice per group. Experiments were repeated 2 or 3 times yielding similar results. *p < 0.001–0.05 by Student’s t test performed between two groups. One-way ANOVA followed by Tukey’s post hoc test was performed among three or more groups.

the energy state of MODCs. Although PPAR γ is known for its properties in mitochondrial biogenesis, we found that mitochondria are disrupted in MODCs, which may be a product of itaconate’s effects on mitochondrial metabolism. Thus, we hypothesize that PPAR γ activation contributes to the availability of glucose/pyruvate and fatty acids that feed the synthesis of derivatives of the TCA cycle, as aconitate and itaconate affect mitochondria’s viability.⁴² In fact, we have previously described an association between disrupted mitochondrial metabolism in monocytes and symptomatic infection in humans and mice.^{8,43} Accordingly, previous studies showed that *P. falciparum*- and *P. vivax*-infected

stimulation of Toll-like receptors (TLRs) and cytosolic sensors by parasite components (e.g., DNA, RNA, and hemozoin), primed monocytes release high levels of pro-inflammatory cytokines,^{35–37} leading to systemic inflammation and signs of disease.³⁸ Here, we report that, while inducing the differentiation of MODCs, IFN γ promotes glycolysis, leading to a mitochondrial state that accumulates TCA cycle-derived itaconate. IFN γ signaling also induces PPAR γ expression in MODCs of infected mice. PPAR γ activation promotes fatty acid oxidation and glucose uptake—both of which are relevant pathways for MODC differentiation and maturation.^{39–41} It is unclear whether PPAR γ is directly induced by transcriptional factors of the IFN γ pathway, or if enhanced expression of PPAR γ is a consequence of the gene signature in differentiated MODCs. Nevertheless, our results indicate an important role of PPAR γ on

patients have impaired DC maturation and antigen presentation to T cells.^{38,44,45} Consistently, He et al. demonstrated that *in vitro* exogenous treatment of lipopolysaccharide (LPS)-stimulated macrophages with itaconate limits antigen presentation and lymphocyte activation.²⁷

When itaconate accumulates intra- and extracellularly, it exerts different roles in the interactions between the host and pathogen: (1) itaconate can be an antimicrobial metabolite⁴⁶; (2) it has stimulatory effects on host enzymes that can detrimental to the pathogen^{19,46}; or (3) it has immunoregulatory properties that can promote host susceptibility to infection.¹⁹ To our knowledge, there is no evidence of a direct or indirect detrimental effect of itaconate synthesis on the *Plasmodium* parasite.⁴⁷ Importantly, we found that the itaconate-free *Acod1*^{-/-} mice show enhanced levels of pro-inflammatory cytokines, low levels of PD-L1

expression, and enhanced resistance to *Pc* infection relative to WT mice. Thus, we hypothesize that the itaconate immunoregulatory effects on the host are the most relevant for disease development in this model. Recently, a report demonstrated that itaconate can generate secondary metabolites. Mesaconate derived from itaconate phenocopies the immunoregulatory effects of itaconate.²⁷ Here, for the first time, we demonstrated that mesaconate can be synthesized *in vivo* and *ex vivo* by myeloid cells in a pathological context. In our analysis, we found that itaconate and mesaconate are the only TCA cycle-derived metabolites that accumulate in the plasma of infected mice, and they may act together to regulate host immune responses. However, the concentration of mesaconate was around one fourth of the itaconate concentration, suggesting an adjuvant immunoregulatory role.

Exogenous itaconate regulates macrophage activation through direct engagement of the NRF2 and ATF3 regulatory pathways that limit the production of type I IFN from LPS-stimulated macrophages^{7,29} while promoting IL-10 release.⁴⁸ In the same *in vitro* model, itaconate treatment delays NLRP3 inflammasome activation in macrophages.^{49,50} Yet, in alternatively activated macrophages (IL-4-induced), exogenous itaconate inhibits JAK1 phosphorylation,⁵¹ which might reduce the activation of cytokines that signal through JAK1, such as IL-6, TNF, and IFN γ .⁵² We found, however, that NRF2 expression was inhibited, whereas ATF3 expression was not altered in CD11b+ cells from *Pc*-infected mice. Nevertheless, we found that κ B ζ , which promotes the release of IL-6 and TNF by monocytes, is inhibited by itaconate in MODCs of infected mice. Thus, we speculate whether suppressive effects of itaconate on MODCs could protect the host from deleterious systemic inflammation in models of lethal malaria.

Importantly, immune suppression in malaria can be induced by IRF7 activation and type I IFN signaling.⁵³ The recognition of nucleic acids by cytosolic sensors activates IRF3 and IRF7, which sustains the expression of ISGs and type I IFN signaling. In studies performed by our group and elsewhere, it was shown that *Plasmodium* nucleic acids are sensed by cGAS and other cytosolic receptors in macrophages.^{30,54–56} Nonetheless, recent findings show that mitochondrial damage can release mtDNA in cytosol, which induce the expression of checkpoint markers in IRF3/7-dependent way.^{32,33} In addition, there is an extensive literature showing the importance of IFN γ in priming monocytes during *Plasmodium* infection,^{17,38,57} corroborating the hypothesis that IFN γ signaling initiates the expression of ISGs in MODCs, which is sustained by cytosolic sensing of mtDNA. Our data on the mitochondria's damage suggest that during *Plasmodium* infection, itaconate accumulation induced by the IFN γ /PPAR γ axis disrupts the TCA cycle in MODCs, damaging mitochondria and causing release of mitochondrial genome fragments into the cytosol. Once sensed by a cytosolic innate immune receptor, potentially cGAS, the fragments of the mitochondrial genome trigger PD-L1 expression via the STING/IRF3/IRF7 pathway. This hypothesis is consistent with the findings that accumulation of fumarate due to deficiency of the TCA enzyme fumarate hydratase, as well as inhibition of *de novo* synthesis of nucleotides, lead to cytosolic leakage of mtDNA and activation of cGAS-STING-TBK1.^{58,59} Alternatively, we found that expression of RIG-I and MDA5 is augmented in MODCs, suggesting that mtdsRNA

may also contribute to IRF3/IRF7-induced PD-L1 expression via MAVS activation. Furthermore, we found that *in vitro* priming of MODCs with IFN γ recapitulates the phenotype of MODCs with damaged mitochondria induced during *in vivo* *Pc* infection. We hypothesize that in our model, nucleic acid cytosolic sensors, which ultimately trigger PD-L1 expression on MODCs, are activated by self-mtDNA (or mtdsRNA). Accordingly, CD8+ T cells display an exhausted phenotype induced by PD-L1 resulting in uninhibited growth of blood-stage malaria. Consistently, PD-L1 blockade enhances parasitemia clearance in rodent malaria.⁶⁰ So far, most studies indicate that itaconate's effects on lymphocytes are due to an indirect effect in myeloid cells.^{61–65} Although we did not evaluate the direct effect of endogenous itaconate on CD8+ T cells, ACOD1 is expressed only by myeloid cells. Thus, we assume that the effects of itaconate on CD8+ T cells in our model are indirect due to induction of PD-L1 in MODCs.

In summary, for the first time, we show the importance of itaconate in regulating the immune response and enhanced susceptibility to a parasitic infection. MODCs have an important role in the pathogenesis of both human disease and experimental models of malaria.^{38,66} We now present evidence that the status of activation of these cells is intrinsically linked to mitochondrial function. Consistently, our results show that itaconate promotes host susceptibility to infection. Thus, targeting ACOD1 and limiting itaconate availability could boost immune response against *Plasmodium*, which could improve the efficacy of conventional antimalarial therapies.

Limitations of the study

In our model, cGAS is a prime candidate for sensing mtDNA and activating the STING-IRF3/IRF7 pathway. While we detected high levels of intermediary metabolites that are part of cyclic GMP-AMP (cGAMP) generation, our untargeted metabolomic approach did not detect cGAMP within MODCs. This raises the question regarding the sensitivity of our assay to detect dinucleotides, in particular cGAMP. We also noticed that the proteins RIG-I and MDA5 that sense mtdsRNA show enhanced expression in MODCs from *Pc*-infected mice. Furthermore, different studies indicate that *Plasmodium* infection activates various nucleic acid-sensing cytosolic receptors.⁶⁶ Hence, despite the robust data generated by multiple approaches that indicate a key role for STING, IRF3, and IRF7 in inducing PD-L1, the contribution of RIG-I and MDA5 in promoting PD-L1 expression needs further investigation.

The immune response is a double-edged sword during malaria. CD8 T cells are implicated in host resistance to the blood stage of *P. vivax* malaria in humans and in other malaria mouse model.^{67,68} However, CD8 T cells can also be pathogenic, for instance in the cerebral experimental malaria.^{69,70} Our results show that itaconate impairs control of parasitemia by limiting CD8 T cell function during the acute phase of infection. It remains to be defined whether the immune regulatory role of itaconate on systemic inflammation and CD8 T cell function mediates tolerance to disease in the different models of malaria. Thus, as the host condition influences immunity and pathology, further investigation of the effects of endogenous itaconate *in vivo* may provide new insights to intervene in patients with malaria.

STAR★METHODS

Detailed methods are provided in the online version of this paper and include the following:

- **KEY RESOURCES TABLE**
- **RESOURCE AVAILABILITY**
 - Lead contact
 - Materials availability
 - Data and code availability
- **EXPERIMENTAL MODEL AND SUBJECT DETAILS**
 - Ethics for animal experiments and human samples
 - Experimental infections
 - Monocyte-derived dendritic cells (MODCs)
 - Stimulation of immortalized bone marrow-derived macrophages with IFN γ
- **METHOD DETAILS**
 - Glucose uptake in total splenocytes
 - Flow cytometry in total splenocytes
 - Cytokine detection in plasma and supernatant samples
 - Western blotting
 - Pharmacological inhibitors
 - Transcriptomes in total splenocytes
 - Untargeted and targeted metabolome of MODCs
 - Untargeted lipidome of MODCs
 - Transcriptome profiling of monocytes from patients infected with *P. vivax*
 - Public metabolomics and transcriptomics analyses
 - Oxygen consumption rate and extracellular acidification in MODCs
- **QUANTIFICATION AND STATISTICAL ANALYSIS**

SUPPLEMENTAL INFORMATION

Supplemental information can be found online at <https://doi.org/10.1016/j.cmet.2024.01.008>.

ACKNOWLEDGMENTS

This work was supported by the US NIH (R01NS098747, R01AI079293, and R21 AI150546), the Brazilian National Institute of Science and Technology for Vaccines (INCT/CNPq), the Fundação de Pesquisa do Estado de Minas Gerais (465293/2014-0), and the Fundação de Amparo de Pesquisa do Estado de Sao Paulo (2016/23618-8). Our sorting assays were supported by NIH grant S10 S10OD028576. Hira Goel kindly performed the western blots showing the expression of ATF3 and NRF2 (Figures S5E and S5F). iBMDMs were previously generated by Rosane de Oliveira while working in the Golenbock laboratory. Gail Germain and Heather Farineau maintained the mice lineages used in this study. Kristen Halmen managed all the orders for the materials used in this work. Melanie Trombly kindly edited the text. The schemes and illustrations presented in this study were generated by BioRender.com.

AUTHOR CONTRIBUTIONS

T.R. and R.T.G. elaborated the hypothesis and aims of the study. T.R., P.A.A., O.O., B.C., and O.C. designed and performed the experiments and analyzed the data. L.T. and P.L.L. performed and analyzed targeted and untargeted metabolomics. L.G. analyzed deposited RNA-seq and metabolomics data from human and mouse samples. T.R. and R.T.G. wrote and revised the manuscript. K.A.F., C.H., and D.T.G. elaborated the hypothesis and critically discussed the itaconate mechanisms in this work. R.T.G. and D.T.G. supervised the project. All authors reviewed and approved the final manuscript.

DECLARATION OF INTERESTS

The authors declare no competing interests.

Received: February 8, 2023

Revised: October 27, 2023

Accepted: January 14, 2024

Published: February 6, 2024

REFERENCES

1. Monroe, A., Williams, N.A., Ogoma, S., Karema, C., and Okumu, F. (2022). Reflections on the 2021 World Malaria Report and the future of malaria control. *Malar. J.* *21*, 154.
2. Schofield, L., and Grau, G.E. (2005). Immunological processes in malaria pathogenesis. *Nat. Rev. Immunol.* *5*, 722–735.
3. Clark, I.A., Budd, A.C., Alleva, L.M., and Cowden, W.B. (2006). Human malarial disease: a consequence of inflammatory cytokine release. *Malar. J.* *5*, 85.
4. Pålsson-McDermott, E.M., and O'Neill, L.A.J. (2020). Targeting immunometabolism as an anti-inflammatory strategy. *Cell Res.* *30*, 300–314.
5. Martínez-Reyes, I., and Chandel, N.S. (2020). Mitochondrial TCA cycle metabolites control physiology and disease. *Nat. Commun.* *11*, 102.
6. Choi, I., Son, H., and Baek, J.H. (2021). Tricarboxylic Acid (TCA) Cycle Intermediates: Regulators of Immune Responses. *Life (Basel)* *11*, 69.
7. Mills, E.L., Ryan, D.G., Prag, H.A., Dikovskaya, D., Menon, D., Zaslona, Z., Jedrychowski, M.P., Costa, A.S.H., Higgins, M., Hams, E., et al. (2018). Itaconate is an anti-inflammatory metabolite that activates Nrf2 via alkylation of KEAP1. *Nature* *556*, 113–117.
8. Diniz, S.Q., Teixeira-Carvalho, A., Figueiredo, M.M., Costa, P.A.C., Rocha, B.C., Martins-Filho, O.A., Gonçalves, R., Pereira, D.B., Tada, M.S., Oliveira, F., et al. (2021). Plasmodium vivax Infection Alters Mitochondrial Metabolism in Human Monocytes. *mBio* *12*, e0124721.
9. Vijay, R., Guthmiller, J.J., Sturtz, A.J., Surette, F.A., Rogers, K.J., Sompallae, R.R., Li, F., Pope, R.L., Chan, J.A., de Labastida Rivera, F., et al. (2020). Infection-induced plasmablasts are a nutrient sink that impairs humoral immunity to malaria. *Nat. Immunol.* *21*, 790–801.
10. Gordon, E.B., Hart, G.T., Tran, T.M., Waisberg, M., Akkaya, M., Kim, A.S., Hamilton, S.E., Pena, M., Yazew, T., Qi, C.F., et al. (2015). Targeting glutamine metabolism rescues mice from late-stage cerebral malaria. *Proc. Natl. Acad. Sci. USA* *112*, 13075–13080.
11. Cordy, R.J., Patrapuvich, R., Lili, L.N., Cabrera-Mora, M., Chien, J.T., Tharp, G.K., Khadka, M., Meyer, E.V., Lapp, S.A., Joyner, C.J., et al. (2019). Distinct amino acid and lipid perturbations characterize acute versus chronic malaria. *JCI Insight* *4*, e125156.
12. Gardinassi, L.G., Cordy, R.J., Lacerda, M.V.G., Salinas, J.L., Monteiro, W.M., Melo, G.C., Siqueira, A.M., Val, F.F., Tran, V., Jones, D.P., et al. (2017). Metabolome-wide association study of peripheral parasitemia in Plasmodium vivax malaria. *Int. J. Med. Microbiol.* *307*, 533–541.
13. Pappa, V., Seydel, K., Gupta, S., Feintuch, C.M., Potchen, M.J., Kampondeni, S., Goldman-Yassen, A., Veenstra, M., Lopez, L., Kim, R.S., et al. (2015). Lipid metabolites of the phospholipase A2 pathway and inflammatory cytokines are associated with brain volume in paediatric cerebral malaria. *Malar. J.* *14*, 513.
14. Colvin, H.N., and Joice Cordy, R. (2020). Insights into malaria pathogenesis gained from host metabolomics. *PLoS Pathog.* *16*, e1008930.
15. Antonelli, L.R.V., Leoratti, F.M.S., Costa, P.A.C., Rocha, B.C., Diniz, S.Q., Tada, M.S., Pereira, D.B., Teixeira-Carvalho, A., Golenbock, D.T., Gonçalves, R., et al. (2014). The CD14+CD16+ inflammatory monocyte subset displays increased mitochondrial activity and effector function during acute Plasmodium vivax malaria. *PLoS Pathog.* *10*, e1004393.
16. Hirako, I.C., Assis, P.A., Hojo-Souza, N.S., Reed, G., Nakaya, H., Golenbock, D.T., Coimbra, R.S., and Gazzinelli, R.T. (2018). Daily Rhythms of TNF α Expression and Food Intake Regulate Synchrony of

- Plasmodium Stages with the Host Circadian Cycle. *Cell Host Microbe* 23, 796–808.e6.
17. Hirako, I.C., Ataíde, M.A., Faustino, L., Assis, P.A., Sorensen, E.W., Ueta, H., Araújo, N.M., Menezes, G.B., Luster, A.D., and Gazzinelli, R.T. (2016). Splenic differentiation and emergence of CCR5+CXCL9+CXCL10+ monocyte-derived dendritic cells in the brain during cerebral malaria. *Nat. Commun.* 7, 13277.
 18. Assis, P.A., Fernandes Durso, D., Chacon Cavalcante, F., Zaniratto, R., Carvalho-Silva, A.C., Cunha-Neto, E., Golenbock, D.T., Rodrigues Pinto Ferreira, L., and Tostes Gazzinelli, R. (2020). Integrative analysis of microRNA and mRNA expression profiles of monocyte-derived dendritic cells differentiation during experimental cerebral malaria. *J. Leukoc. Biol.* 108, 1183–1197.
 19. Peace, C.G., and O'Neill, L.A. (2022). The role of itaconate in host defense and inflammation. *J. Clin. Invest.* 132, e148548.
 20. Lampropoulou, V., Sergushichev, A., Bambouskova, M., Nair, S., Vincent, E.E., Loginicheva, E., Cervantes-Barragan, L., Ma, X., Huang, S.C.-C., Griss, T., et al. (2016). Itaconate Links Inhibition of Succinate Dehydrogenase with Macrophage Metabolic Remodeling and Regulation of Inflammation. *Cell Metab.* 24, 158–166.
 21. Pettus, B.J., Chalfant, C.E., and Hannun, Y.A. (2002). Ceramide in apoptosis: an overview and current perspectives. *Biochim. Biophys. Acta* 1585, 114–125.
 22. Nagata, S., Suzuki, J., Segawa, K., and Fujii, T. (2016). Exposure of phosphatidylserine on the cell surface. *Cell Death Differ.* 23, 952–961.
 23. Pizzuto, M., and Pelegrin, P. (2020). Cardiolipin in Immune Signaling and Cell Death. *Trends Cell Biol.* 30, 892–903.
 24. Picard, F., and Auwerx, J. (2002). PPAR γ AND G LUCOSE HOMEOSTASIS. *Annu. Rev. Nutr.* 22, 167–197.
 25. Barber, D.L., Wherry, E.J., Masopust, D., Zhu, B., Allison, J.P., Sharpe, A.H., Freeman, G.J., and Ahmed, R. (2006). Restoring function in exhausted CD8 T cells during chronic viral infection. *Nature* 439, 682–687.
 26. Hou, Y., Moreau, F., and Chadee, K. (2012). PPAR γ is an E3 ligase that induces the degradation of NF κ B/p65. *Nat. Commun.* 3, 1300.
 27. He, W., Henne, A., Lauterbach, M., Geißmar, E., Nikolka, F., Kho, C., Heinz, A., Dostert, C., Grusdat, M., Cordes, T., et al. (2022). Mesaconate is synthesized from itaconate and exerts immunomodulatory effects in macrophages. *Nat. Metab.* 4, 524–533.
 28. Wang, S.F., Adler, J., and Lardy, H.A. (1961). The pathway of itaconate metabolism by liver mitochondria. *J. Biol. Chem.* 236, 26–30.
 29. Bambouskova, M., Gorvel, L., Lampropoulou, V., Sergushichev, A., Loginicheva, E., Johnson, K., Korenfeld, D., Mathyer, M.E., Kim, H., Huang, L.H., et al. (2018). Electrophilic properties of itaconate and derivatives regulate the I κ B ζ -ATF3 inflammatory axis. *Nature* 556, 501–504.
 30. Sun, L., Wu, J., Du, F., Chen, X., and Chen, Z.J. (2013). Cyclic GMP-AMP synthase is a cytosolic DNA sensor that activates the type I interferon pathway. *Science* 339, 786–791.
 31. Dhir, A., Dhir, S., Borowski, L.S., Jimenez, L., Teitell, M., Rötig, A., Crow, Y.J., Rice, G.I., Duffy, D., Tamby, C., et al. (2018). Mitochondrial double-stranded RNA triggers antiviral signalling in humans. *Nature* 560, 238–242.
 32. Tigano, M., Vargas, D.C., Tremblay-Belzile, S., Fu, Y., and Sfeir, A. (2021). Nuclear sensing of breaks in mitochondrial DNA enhances immune surveillance. *Nature* 591, 477–481.
 33. Cheng, A.N., Cheng, L.C., Kuo, C.L., Lo, Y.K., Chou, H.Y., Chen, C.H., Wang, Y.H., Chuang, T.H., Cheng, S.J., and Lee, A.Y.-L. (2020). Mitochondrial Lon-induced mtDNA leakage contributes to PD-L1-mediated immunoescape via STING-IFN signaling and extracellular vesicles. *J. Immunother. Cancer* 8, e001372.
 34. Galvão-Filho, B., de Castro, J.T., Figueiredo, M.M., Rosmaninho, C.G., Antonelli, L.R.D.V., and Gazzinelli, R.T. (2019). The emergence of pathogenic TNF/INOS producing dendritic cells (Tip-DCs) in a malaria model of acute respiratory distress syndrome (ARDS) is dependent on CCR4. *Mucosal Immunol.* 12, 312–322.
 35. Ataíde, M.A., Andrade, W.A., Zamboni, D.S., Wang, D., Souza, M.do C., Franklin, B.S., Elian, S., Martins, F.S., Pereira, D., Reed, G., et al. (2014). Malaria-induced NLRP12/NLRP3-dependent caspase-1 activation mediates inflammation and hypersensitivity to bacterial superinfection. *PLoS Pathog.* 10, e1003885.
 36. Hirako, I.C., Gallego-Marin, C., Ataíde, M.A., Andrade, W.A., Gravina, H., Rocha, B.C., de Oliveira, R.B., Pereira, D.B., Vinetz, J., Diamond, B., et al. (2015). DNA-Containing Immunocomplexes Promote Inflammasome Assembly and Release of Pyrogenic Cytokines by CD14+ CD16+ CD64high CD32low Inflammatory Monocytes from Malaria Patients. *mBio* 6, e01605–e01615.
 37. Kalantari, P., DeOliveira, R.B., Chan, J., Corbett, Y., Rathinam, V., Stutz, A., Latz, E., Gazzinelli, R.T., Golenbock, D.T., and Fitzgerald, K.A. (2014). Dual engagement of the NLRP3 and AIM2 inflammasomes by plasmodium-derived hemozoin and DNA during malaria. *Cell Rep.* 6, 196–210.
 38. Hirako, I.C., Assis, P.A., Galvão-Filho, B., Luster, A.D., Antonelli, L.R., and Gazzinelli, R.T. (2019). Monocyte-derived dendritic cells in malaria. *Curr. Opin. Microbiol.* 52, 139–150.
 39. Szatmari, I., Gogolak, P., Im, J.S., Dezso, B., Rajnavolgyi, E., and Nagy, L. (2004). Activation of PPAR γ specifies a dendritic cell subtype capable of enhanced induction of iNKT cell expansion. *Immunity* 21, 95–106.
 40. Szatmari, I., Töröcsik, D., Agostini, M., Nagy, T., Gurnell, M., Barta, E., Chatterjee, K., and Nagy, L. (2007). PPAR γ regulates the function of human dendritic cells primarily by altering lipid metabolism. *Blood* 110, 3271–3280.
 41. Nencioni, A., Grünebach, F., Zobywalski, A., Denzlinger, C., Brugger, W., and Brossart, P. (2002). Dendritic cell immunogenicity is regulated by peroxisome proliferator-activated receptor gamma. *J. Immunol.* 169, 1228–1235.
 42. Adamik, J., Munson, P.V., Hartmann, F.J., Combes, A.J., Pierre, P., Krummel, M.F., Bendall, S.C., Argüello, R.J., and Butterfield, L.H. (2022). Distinct metabolic states guide maturation of inflammatory and tolerogenic dendritic cells. *Nat. Commun.* 13, 5184.
 43. Dos Santos, L.I., Torres, T.A., Diniz, S.Q., Gonçalves, R., Caballero-Flores, G., Núñez, G., Gazzinelli, R.T., Maloy, K.J., and Ribeiro do V Antonelli, L. (2021). Disrupted Iron Metabolism and Mortality during Co-infection with Malaria and an Intestinal Gram-Negative Extracellular Pathogen. *Cell Rep.* 34, 108613.
 44. Costa, P.A.C., Leoratti, F.M.S., Figueiredo, M.M., Tada, M.S., Pereira, D.B., Junqueira, C., Soares, I.S., Barber, D.L., Gazzinelli, R.T., and Antonelli, L.R.V. (2015). Induction of Inhibitory Receptors on T Cells During Plasmodium vivax Malaria Impairs Cytokine Production. *J. Infect. Dis.* 212, 1999–2010.
 45. Wykes, M.N., and Good, M.F. (2008). What really happens to dendritic cells during malaria? *Nat. Rev. Microbiol.* 6, 864–870.
 46. Luan, H.H., and Medzhitov, R. (2016). Food Fight: Role of Itaconate and Other Metabolites in Antimicrobial Defense. *Cell Metab.* 24, 379–387.
 47. Olszewski, K.L., Mather, M.W., Morrisey, J.M., Garcia, B.A., Vaidya, A.B., Rabinowitz, J.D., and Linás, M. (2013). Retraction: Branched tricarboxylic acid metabolism in Plasmodium falciparum. *Nature* 497, 652.
 48. Sun, Q., Hu, T., Zhang, Y., Wang, X., Liu, J., Chen, W., Wei, C., Liu, D., Wu, W., Lan, T., et al. (2022). IRG1/itaconate increases IL-10 release to alleviate mechanical and thermal hypersensitivity in mice after nerve injury. *Front. Immunol.* 13, 1012442.
 49. Hooftman, A., Angiari, S., Hester, S., Corcoran, S.E., Runtsch, M.C., Ling, C., Ruzek, M.C., Slivka, P.F., McGettrick, A.F., Banahan, K., et al. (2020). The Immunomodulatory Metabolite Itaconate Modifies NLRP3 and Inhibits Inflammasome Activation. *Cell Metab.* 32, 468–478.e7.
 50. Bambouskova, M., Potuckova, L., Paulenda, T., Kerndl, M., Mogilenko, D.A., Lizotte, K., Swain, A., Hayes, S., Sheldon, R.D., Kim, H., et al. (2021). Itaconate confers tolerance to late NLRP3 inflammasome activation. *Cell Rep.* 34, 108756.

51. Runtsch, M.C., Angiari, S., Hooftman, A., Wadhwa, R., Zhang, Y., Zheng, Y., Spina, J.S., Ruzek, M.C., Argiriadi, M.A., McGettrick, A.F., et al. (2022). Itaconate and itaconate derivatives target JAK1 to suppress alternative activation of macrophages. *Cell Metab.* *34*, 487–501.e8.
52. Schindler, C., Levy, D.E., and Decker, T. (2007). JAK-STAT signaling: from interferons to cytokines. *J. Biol. Chem.* *282*, 20059–20063.
53. Edwards, C.L., Best, S.E., Gun, S.Y., Claser, C., James, K.R., de Oca, M.M., Sebina, I., Rivera, F.de L., Amante, F.H., Hertzog, P.J., et al. (2015). Spatiotemporal requirements for IRF7 in mediating type I IFN-dependent susceptibility to blood-stage Plasmodium infection. *Eur. J. Immunol.* *45*, 130–141.
54. Wu, J., Tian, L., Yu, X., Pattaradilokrat, S., Li, J., Wang, M., Yu, W., Qi, Y., Zeituni, A.E., Nair, S.C., et al. (2014). Strain-specific innate immune signaling pathways determine malaria parasitemia dynamics and host mortality. *Proc. Natl. Acad. Sci. USA* *111*, E511–E520.
55. He, X., Xia, L., Tumas, K.C., Wu, J., and Su, X.Z. (2020). Type I Interferons and Malaria: A Double-Edge Sword Against a Complex Parasitic Disease. *Front. Cell. Infect. Microbiol.* *10*, 594621.
56. Yu, X., Cai, B., Wang, M., Tan, P., Ding, X., Wu, J., Li, J., Li, Q., Liu, P., Xing, C., et al. (2016). Cross-Regulation of Two Type I Interferon Signaling Pathways in Plasmacytoid Dendritic Cells Controls Anti-malaria Immunity and Host Mortality. *Immunity* *45*, 1093–1107.
57. Crabtree, J.N., Caffrey, D.R., de Souza Silva, L., Kurt-Jones, E.A., Dobbs, K., Dent, A., Fitzgerald, K.A., and Golenbock, D.T. (2022). Lymphocyte crosstalk is required for monocyte-intrinsic trained immunity to Plasmodium falciparum. *J. Clin. Invest.* *132*, e139298.
58. Zecchini, V., Paupe, V., Herranz-Montoya, I., Janssen, J., Wortel, I.M.N., Morris, J.L., Ferguson, A., Chowdury, S.R., Segarra-Mondejar, M., Costa, A.S.H., et al. (2023). Fumarate induces vesicular release of mtDNA to drive innate immunity. *Nature* *615*, 499–506.
59. Sprenger, H.G., MacVicar, T., Bahat, A., Fiedler, K.U., Hermans, S., Ehrentraut, D., Ried, K., Milenkovic, D., Bonekamp, N., Larsson, N.G., et al. (2021). Cellular pyrimidine imbalance triggers mitochondrial DNA-dependent innate immunity. *Nat. Metab.* *3*, 636–650.
60. Butler, N.S., Moebius, J., Pewe, L.L., Traore, B., Doumbo, O.K., Tygrett, L.T., Waldschmidt, T.J., Crompton, P.D., and Harty, J.T. (2011). Therapeutic blockade of PD-L1 and LAG-3 rapidly clears established blood-stage Plasmodium infection. *Nat. Immunol.* *13*, 188–195.
61. Jaiswal, A.K., Yadav, J., Makhija, S., Mazumder, S., Mitra, A.K., Suryawanshi, A., Sandey, M., and Mishra, A. (2022). Irg1/itaconate metabolic pathway is a crucial determinant of dendritic cells immune-priming function and contributes to resolute allergen-induced airway inflammation. *Mucosal Immunol.* *15*, 301–313.
62. Zhao, H., Teng, D., Yang, L., Xu, X., Chen, J., Jiang, T., Feng, A.Y., Zhang, Y., Frederick, D.T., Gu, L., et al. (2022). Myeloid-derived itaconate suppresses cytotoxic CD8+ T cells and promotes tumour growth. *Nat. Metab.* *4*, 1660–1673.
63. Chen, Y.J., Li, G.N., Li, X.J., Wei, L.X., Fu, M.J., Cheng, Z.L., Yang, Z., Zhu, G.Q., Wang, X.D., Zhang, C., et al. (2023). Targeting IRG1 reverses the immunosuppressive function of tumor-associated macrophages and enhances cancer immunotherapy. *Sci. Adv.* *9*, eadg0654.
64. Roberts, L.M., Leighton, I., Schwarz, B., Wehrly, T.D., Evans, T.J., and Bosio, C.M. (2022). Itaconate indirectly influences expansion of effector T cells following vaccination with Francisella tularensis live vaccine strain. *Cell. Immunol.* *373*, 104485.
65. Sohail, A., Iqbal, A.A., Sahini, N., Chen, F., Tantawy, M., Waqas, S.F.H., Winterhoff, M., Ebensen, T., Schultz, K., Geffers, R., et al. (2022). Itaconate and derivatives reduce interferon responses and inflammation in influenza A virus infection. *PLoS Pathog.* *18*, e1010219.
66. Gazzinelli, R.T., Kalantari, P., Fitzgerald, K.A., and Golenbock, D.T. (2014). Innate sensing of malaria parasites. *Nat. Rev. Immunol.* *14*, 744–757.
67. Hojo-Souza, N.S., de Azevedo, P.O., de Castro, J.T., Teixeira-Carvalho, A., Lieberman, J., Junqueira, C., and Gazzinelli, R.T. (2020). Contributions of IFN- γ and granulysin to the clearance of Plasmodium yoelii blood stage. *PLoS Pathog.* *16*, e1008840.
68. Junqueira, C., Barbosa, C.R.R., Costa, P.A.C., Teixeira-Carvalho, A., Castro, G., Sen Santara, S., Barbosa, R.P., Dotiwala, F., Pereira, D.B., Antonelli, L.R., et al. (2018). Cytotoxic CD8+ T cells recognize and kill Plasmodium vivax-infected reticulocytes. *Nat. Med.* *24*, 1330–1336.
69. Riggall, B.A., Manglani, M., Maric, D., Johnson, K.R., Lee, M.H., Neto, O.L.A., Taylor, T.E., Seydel, K.B., Nath, A., Miller, L.H., et al. (2020). CD8+ T cells target cerebrovasculature in children with cerebral malaria. *J. Clin. Invest.* *130*, 1128–1138.
70. Belnoue, E., Kayibanda, M., Vigario, A.M., Deschemin, J.C., van Rooijen, N., Viguier, M., Snounou, G., and R nia, L. (2002). On the pathogenic role of brain-sequestered alphabeta CD8+ T cells in experimental cerebral malaria. *J. Immunol.* *169*, 6369–6375.

STAR★METHODS

KEY RESOURCES TABLE

REAGENT or RESOURCE	SOURCE	IDENTIFIER
Antibodies		
Anti-F480 (clone BM8) – PE-Cy5	Thermo Fischer	15-4801-82; RRID: AB_468798
Anti-CD11b (clone M1/70) - PE-Cy7	Invitrogen	25-0112-81; RRID: AB_469587
Anti-CD209a (clone MMD3) - eFluor660	eBioscience	50-2094-82; RRID: AB_11219065
Anti-MHCII I-A(b) PE (clone AF6-120.1) - PE	BD	553552; RRID: AB_394919
Anti-CD86 (B7-2) (clone GL1) - Super Bright 702	eBioscience	67-0862-82; RRID: AB_2717155
Anti-CD80 (B7-1) (clone 16-10A1) – FITC	eBioscience	11-0801-82; RRID: AB_465133
anti-CD274 (PD-L1) (clone MIH5) - Super Bright 600	eBioscience	63-5982-82; RRID: AB_2688101
Anti-CD11c (clone N418) - Alexa Fluor 700	Invitrogen	56-0114-82; RRID: AB_493992
Anti-Tbet (clone eBio4B10) – PE	Thermo Fischer	12-5825-82; RRID: AB_925761
Anti-CD3 (clone 17A2) - PE-eFluor619	eBioscience	61-0032-82; RRID: AB_2815286
Anti-IFN γ (clone XMG1.2) - eFluor660	eBioscience	17-7311-82; RRID: AB_469504
Anti-CD4 (clone GK1.5) - Alexa Fluor700	eBioscience	56-0041-82; RRID: AB_493999
Anti-CD8 mouse (clone 53-6.7) - APC-Cy7	Biolegend	100714; RRID: AB_312753
Anti-CXCR3 (clone CXCR3-173) BV421	BD	566283; RRID: AB_2739657
Anti-GLUT1 (clone EPR3915) - Alexa Fluor 405	Abcam	ab210438; RRID: AB_2895210
Anti-GLUT1 Rat (clone SPM498)	Abcam	Ab40084; RRID: AB_2190927
Anti-ATF3 mouse (clone 44c3a)	Santa Cruz	sc-81189; RRID: AB_2058591
Anti-Ik β mouse	Cell signaling	93726; RRID: AB_2800211
Anti-NRF2 Rabbit (clone D1Z9C)	Cell signaling	12721; RRID: AB_2715528
Anti-PPAR γ mouse (E-8)	Santa Cruz	SC-7273; RRID: AB_628115
Anti-ACOD1 mouse (IRG1)	Cell Signaling	17805; RRID: AB_3064865
Chemicals, peptides, and recombinant proteins		
GW9662	Sigma	M6191
Etomoxir	Sigma	E1905
Recombinant mouse IFN γ	Biolegend	575308
2-cyano-3, 12-dioxooleana-1,9-dien-28-oic acid (CDDO)	Cayman	11883
4-octyl itaconate	Sigma	SML2338
UK-5099	Sigma	PZ0160
Cell Stimulation Cocktail 500x	Thermo Fischer	00-4975-03
D-galactose	Sigma	G5388
6-diazo-5-oxo-L-norleucine (DON)	Sigma	D2141
2-deoxy-D-glucose	Sigma	D8375
Critical commercial assays		
FIX&PERM kit	Thermo Fischer	GAS001S100
CBA mouse inflammation kit	BD	552364
MitoStress Kit	Agilent	103015100
Mouse PD-L1 DuoSet ELISA	R&D	DY1019
Mouse CCL5/RANTES DuoSet ELISA	R&D	DY478
Deposited data		
RNAseq in monocytes from children during acute malaria caused by <i>P. falciparum</i>	NCBI GEO Datasets	GSE154317

(Continued on next page)

Continued

REAGENT or RESOURCE	SOURCE	IDENTIFIER
RNAseq in human monocytes stimulated with <i>P. falciparum</i> -infected red blood cells (iRBC)	NCBI GEO Datasets	GSE151116
RNAseq in MODCs from non-infected and PbA-infected mice	NCBI GEO Datasets	GSE126381
RNAseq in monocytes from non-infected and <i>P. vivax</i> -infected individuals	Zenodo.org (openaire)	7683361
Non-targeted metabolomics in plasma from mice infected with <i>P. chabaudi</i>	Metabolomics Workbench	ST001775
Non-targeted metabolomics in plasma from human infected with <i>P. vivax</i>	MetaboLights	MTBLS665
Non-targeted metabolomics/lipidomics in MODC from Pc-infected mice	Zenodo.org (openaire)	7608255
Unprocessed data for graphs in main figures	This paper	Data S1
Unprocessed data for graphs in Figures S1–S6	This paper	Data S1
Uncropped western blot images	This paper	Data S1
Experimental models: Cell lines		
iBMDM from WT mice	Prof. Douglas Golenbock	This paper
iBMDM from IRF7 ^{-/-} mice	Prof. Douglas Golenbock	This paper
iBMDM from IRF3/7 ^{-/-} mice	Prof. Douglas Golenbock	This paper
Experimental models: Organisms/strains		
Mouse: PPARg ^{-/-} LysM-cre	Prof. Ricardo Gazzinelli	This paper
Mouse: IFNgR ^{-/-} LysM-cre	Prof. Ricardo Gazzinelli	This paper
Mouse: ACOD1 ^{-/-}	The Jackson Laboratory	029340
Mouse: C57BL/6NJ WT	The Jackson Laboratory	005304
Mouse: C57BL/6 WT	Prof. Ricardo Gazzinelli	This paper
Mouse: STING ^{-/-}	Prof. Katherine Fitzgerald	This paper
Software and algorithms		
FlowJo	FlowJo LLC	flowjo.com
Graphpad Prism	Graphpad Software	graphpad.com
Morpheus	Broad Institute	software.broadinstitute.org/morpheus/
R studio	Posit	rstudio.com
Other		
MitoTracker Green FM	Invitrogen	M7514
MitoTracker Red FM	Invitrogen	M22425
Ghost Dye Violet 510 (1:250)	Tonbo Biosciences	13-0870-T100
LIVE/DEAD Green fixable	Invitrogen	L23101

RESOURCE AVAILABILITY

Lead contact

Further information and requests for resources and reagents should be directed to the lead contact, Ricardo T. Gazzinelli, and will be fulfilled by the corresponding authors, Theresa Ramalho (theresa.ramalho@umassmed.edu) and Ricardo T. Gazzinelli (ricardo.gazzinelli@umassmed.edu).

Materials availability

This study did not generate new unique reagents.

Data and code availability

The metabolome and lipidome in splenic MODCs from *Pc*-infected mice generated in this study is new data and can be accessed on zenodo.org with the code #7608255. Metabolomics data from the plasma of C57BL/6 mice infected with *Pc* were retrieved from the

Metabolomics Workbench database under accession ID ST001775. Metabolomics data from the plasma of human volunteers experimentally infected with *P. vivax* were acquired from the MetaboLights repository under accession ID MTBLS665. The RNAseq in monocytes from individuals infected with *P. vivax* is new data and can be found on zenodo.org with the code #7683361. The RNAseq in splenic MODCs from *P. berghei Anka* can be obtained on GEO with the code GSE126381, platform GPL19057. RNAseq in monocytes isolated from children, which were later stimulated with *P. falciparum*-infected red blood cells (iRBC) *in vitro*, is GSE151116. RNAseq in monocytes isolated from children during acute and convalescence phase of malaria caused by *P. falciparum* is GSE154317. RNAseq in effector memory CD4⁺ T cells sorted from adult volunteers experimentally infected with *P. falciparum* before infection (baseline) and 6 days after drug treatment is GSE174791. Uncropped scans of all western blots and all raw data used to generate graphs are included in [Data S1](#). Further information and requests for resources and reagents should be directed to the corresponding authors.

EXPERIMENTAL MODEL AND SUBJECT DETAILS

Ethics for animal experiments and human samples

Experiments with mice were conducted according to institutional guidelines for animal ethics and approved by the Institutional Ethics from UMass Chan Medical School (IACUC/202100027). Experiments with human samples followed the protocol reviewed and approved by the Ethical Committees on Human Experimentation from Instituto René Rachou, Fiocruz, and the National Ethical Council (CAAE: 59902816.7.0000.5091).

Experimental infections

The following mouse lineages generated by our laboratory were used in this study: PPAR γ ^{LysM^{Cre}} KO, IFN γ ^{R^{LysM^{Cre}}} KO, IFN γ ^{-/-}, and Acod1^{-/-} lineages were purchased from The Jackson Laboratory (Bar Harbor, ME). The Acod1^{-/-} lineage was backcrossed for at least ten generations into the C57BL/6NJ, and the other lineages were backcrossed with C57BL/6J. All mouse lineages were bred and maintained in microisolators at UMass Chan on a 12 h dark/light cycle, controlled temperature at 68 to 79 °C, and humidity between 30 and 70%. Female and male mice, between 6 and 10 weeks were used in this study. The *Pc* strain was utilized to induce experimental malaria in mice. The strain was maintained in weekly passages between infected C57BL/6 mice. Passages and experimental infections used 10⁵ infected red blood cells diluted in PBS at room temperature. Parasitemia, body weight, and blood glycemia were monitored during the acute phase of the disease. Blood and spleen samples were collected from infected mice 7 days after the infection. Samples from non-infected mice were also collected for control groups.

Monocyte-derived dendritic cells (MODCs)

Spleens from infected and non-infected mice were macerated on a 100 μ m nylon cell strainer with cell culture media. After centrifuging the macerated sample, erythrocytes were lysed, and total splenocytes were washed. Total splenocytes were used for galactose assay, flow cytometry, and glucose uptake assays. A positive selection for CD11b splenocytes was performed to enrich MODC frequency in splenocyte samples. In some experiments, CD11b⁺ splenocytes were incubated *ex vivo* for 4h for collection of supernatants. Incubation *ex vivo* for 1h was also performed for real-time evaluation of extracellular parameters. In parallel, CD11b⁺ cells were stained for MODC sorting and were also processed for protein and RNA extraction. Alternatively, MODCs were differentiated *in vitro*. Total splenocytes from non-infected mice were plated at a density of 4x10⁶. The cells were stimulated with recombinant IFN γ (100 ng/mL) for 24h. After incubation, the cells were collected and analyzed by flow cytometry. For some *ex vivo* experiments, total splenocytes from infected and non-infected mice were plated on glucose media (regular complete DMEM) or galactose media, in which 25 mM of galactose is used in a DMEM glucose-free media. The splenocytes were incubated overnight, and then MODCs were stained with antibodies to analyze the mitochondria's functionality. For *in vitro* experiments, total splenocytes from non-infected mice were stimulated with recombinant IFN γ (100 ng/mL) in glucose or galactose media and then analyzed by flow cytometry.

Stimulation of immortalized bone marrow-derived macrophages with IFN γ

Immortalized bone marrow-derived macrophages were plated at a density of 4x10⁶. The cells were stimulated with recombinant IFN γ (100 ng/mL) for 24h. After incubation, the cells were collected and stained for flow cytometry.

METHOD DETAILS

Glucose uptake in total splenocytes

Total splenocytes from non-infected and infected mice were aliquoted and incubated with the substrate ³H-2DG at room temperature. After 30 min, a stop solution was added to each sample to stop substrate uptake, cells were lysed with 3% perchloric acid, and radioactivity was detected by scintillation counting.

Flow cytometry in total splenocytes

Total splenocytes were stained with antibodies specific for surface and intracellular markers in MODCs and lymphocytes. Four different antibody panels were used in this work. The three panels used to localize the MODC population in the spleen had the following antibodies: Live/Dead Ghost Aqua V510, Anti-F480 (clone BM8) PE-Cy5, -CD11b (clone M1/70) PE-Cy7, -DCSign (clone

MMD3) APC, -MHCII (clone AF6-120.1) PE. To sort MODCs out, we added the anti-CD3 (17A2) FITC to exclude CD3⁺ cells. MODCs that were CD3^{neg} were collected from the BD FACS Aria Fusion. Sorted cells were processed for further omic analysis. To detect mitochondrial functionality in MODCs, we added the probes Mitotracker Green (60 nM) and Mitotracker Red (70 nM). To evaluate the expression of co-stimulatory markers in MODCs, we added the following antibodies: Anti-CD80 (clone 16-10A1) FITC, -CD86 (clone GL1) Super Bright 702, and -PDL1 (clone MIH5) Super Bright 600. Fixation and permeabilization steps were added to the protocol for intracellular staining with Anti-GLUT1 (clone EPR3915) Alexa Fluor 405 in MODCs. The panel to localize lymphocytes in the spleen included the following antibodies for surface markers: Live/Dead Green, Anti-CD3 (clone 17A2) PE-eFluor610, -CD4 (clone GK1.5) Alexa Fluor 700, -CD8 (clone 53-6.7) APC-Cy7, -CXCR3 (clone 178) Brilliant Violet 421 or -PD1 (clone J43) Brilliant Violet 421. For intracellular staining of lymphocytes, fixation and permeabilization were performed for staining with anti-T-bet (clone 4B10) PE, and anti-IFN γ (clone XMG1.2) APC. All the panels included anti-mouse CD16/32 (clone 93). The acquisition of samples with panels for mitochondrial functionality, co-stimulatory markers, and lymphocyte activation was performed on the Cytex Aurora Spectral Cytometer. All the panels included FMO samples to ensure the precise selection of positive populations. The analysis of the FSC files of experimental and compensation samples was performed on FlowJo.

Cytokine detection in plasma and supernatant samples

The detection of cytokines in the supernatant of MODCs and plasma was performed with the BD CBA Mouse Inflammation Kit and ELISA. All procedures followed directions recommended by the manufacturer.

Western blotting

CD11b⁺ splenocytes from infected and non-infected mice were processed for protein extraction with NP40 supplemented with protease and phosphatase inhibitors. After protein quantification, the samples were prepared to be loaded on SDS-PAGE 10% gel. Then, the protein samples were transferred to PVDF or nitrocellulose membranes. The membranes were incubated with primary antibodies anti-GLUT1 (mouse), anti-PPAR γ (mouse), and anti-ACOD1 (rabbit). Anti-actin was used as an endogenous control. Secondary antibodies anti-mouse or -rabbit conjugated with HRP were incubated after washing the primary antibody. HRP chemiluminescence of each target was revealed with the addition of substrates. The signal of the bands was detected with the ChemiDoc Imaging System (BioRad).

Pharmacological inhibitors

For inhibition pre-differentiation, total splenocytes from non-infected mice were incubated *in vitro* with recombinant IFN γ (100 ng/mL) or only DMEM for 24 h (period for MODC differentiation). IFN γ ⁻ or non-stimulated cells were simultaneously treated with GW9662 (GW, 10 μ M). After the incubation, splenocytes were collected and stained for further flow cytometry analysis to determine the differentiation and mitochondrial status of MODCs. For pharmacologic intervention post-MODC differentiation, CD11b⁺ splenocytes from infected and non-infected mice were incubated *ex vivo* with the following individual treatments: UK5099 (UK) 10 μ M to inhibit Mitochondrial Pyruvate Carrier 1 (MPC-1), Etomoxir (Eto, 3 μ M) to inhibit Carnitine Palmitoyl Transferase 1 alpha (CPT1a), 2-Deoxy-D-Glucose (2-DG, 2 mM) to inhibit hexokinase (HK) and consequent pyruvate synthesis from glycolysis, 6-Diazo-5-oxo-L-norleucine (DON, 50 μ M) to inhibit glutamate synthesis, or GW (10 μ M) to inhibit PPAR γ . The cells were incubated for 1 h with the inhibitors in adequate media for extracellular rate assays. To collect supernatants, CD11b⁺ cells were incubated for 4 h *ex vivo* with inhibitors in DMEM supplemented with penicillin, streptomycin, and 10% FBS.

Transcriptomes in total splenocytes

Total splenocytes collected from *Pc*-infected and non-infected WT and IFN γ ⁻ mice at day 6 post-infection were processed for analysis of gene expression using a gene chip from Affymetrix (23,000) transcripts. The expression values of each gene were determined by the average of differences in intensity (perfect match intensity minus mismatch intensity) between its probe pairs. We plotted the fold-change vs. *p*-value of the genes related to the TCA cycle and its derivatives comparing *Pc*-infected mice with non-infected WT mice and comparing *Pc*-infected IFN γ ⁻ mice with *Pc*-infected WT mice.

Untargeted and targeted metabolome of MODCs

An untargeted metabolome analysis was performed in sorted monocytes from non-infected and in sorted MODCs from *Pc*-infected mice. To determine the relative abundance of polar metabolites in the cells, extracts from the cells were prepared and analyzed by ultra-high-resolution mass spectrometry (HRMS). Metabolites were extracted using ice-cold 0.1% Ammonium hydroxide in 80/20 (v/v) methanol/water. Extracts were centrifuged at 17,000g for 5 min at 4 °C, and supernatants were transferred to clean tubes, followed by evaporation to dryness under nitrogen. Dried extracts were reconstituted in deionized water, and 5 μ L was injected for analysis by ion chromatography (IC)-mass spectrometry (MS). IC mobile phase A was water, and mobile phase B was water containing 100 mM KOH. A Thermo Scientific Dionex ICS-5000+ System included a Thermo IonPac AS11 column (4 μ m particle size, 250 x 2 mm) with the column compartment kept at 30 °C. The autosampler tray was chilled to 4 °C. The mobile phase was 250 μ L/min and a gradient from 1 mM to 100 mM KOH was used. The total run time was 60 min. To assist the desolvation for better sensitivity, methanol was delivered by an external pump and combined with the eluant via a low dead volume mixing tee. Data were acquired using a Thermo Orbitrap Fusion Tribrid Mass Spectrometer under ESI negative ionization mode at a resolution of 240,000. The peak area of each compound was normalized using the total peak area of the respective sample. The total peak area of each sample is defined as the sum of

the peak area intensity for all the compounds in that sample. Additionally, for internal standards, acetic acid-13C₂, butyric acid-13C₄, pentanoic acid-13C₂, and propionic acid 13-C₃ were also introduced in data which were used for normalization of respective compounds prior to total peak area normalization. Next-Generation Clustered Heat Map software was used for clustering analysis. Normalized data was median transformed before generating clustering analysis. Metabolite extraction and analysis for metabolomics and lipidomic analysis (next subsection) were performed at the Metabolic Core Facility, at the MD Anderson Cancer Center of the University of Texas, under the grants supported by NIH grants S10OD012304-01 and P30CA016672.

Untargeted lipidome of MODCs

The lipid extraction solvent consisted of ethanol containing 1% 10 mM butylated hydroxytoluene in methanol and 2% Avanti SPLASH® LIPIDOMIX® Mass Spec Standards. We added 200 μ L extraction solvent to cell pellets, samples were vortexed for 10 min, placed on ice for 10 min, and then centrifuged at 4 °C for 10 min at 17,000g. Supernatants were then collected for LC-MS analysis. For the Reverse Phase Liquid Chromatography, the injection volume was 15 μ L. Mobile phase A (MPA) was 60:40 acetonitrile:water with 0.1% formic acid in 10 mM ammonium formate. Mobile phase B (MPB) was 90:9:1 isopropanol:acetonitrile:water with 0.1% formic acid in 10 mM ammonium formate. The chromatographic method included a Thermo Fisher Scientific Accucore C30 column (2.6 μ m, 150 x 2.1 mm) maintained at 40 °C, a mobile phase flow rate of 0.200 mL/min, and a gradient elution program as follows: 0–3 min, 30% MPB; 3–13 min, 30–43% MPB; 13.1–33 min, 50–70% MPB; 33–48 min, 70–99% MPB; 48–55 min, 99% MPB; 55.1–60 min, 30% MPB. A Thermo Fisher Scientific Orbitrap Fusion Lumos Tribrid mass spectrometer with a heated electrospray ionization source was operated in data-dependent acquisition mode, in both positive and negative ionization modes, with scan ranges of 150–827 and 825–1500 m/z. Orbitrap resolution of 120,000 (FWHM) was used for MS1 acquisition, and spray voltages of 3,600 and -2900 V were used for positive and negative ionization modes, respectively. For MS2 and MS3 fragmentation, a hybridized HCD/CID approach was used. Each sample was analyzed using 4 x 15 μ L injections making use of the two aforementioned scan ranges and ionization modes. Data were analyzed using Thermo Scientific LipidSearch software (version 5.0.63) and processed further using in-house R scripts.

Transcriptome profiling of monocytes from patients infected with *P. vivax*

Patients from the Tropical Medicine Center in Porto Velho (Brazil) were diagnosed with malaria by clinical symptoms and thick blood smear. Five individuals between 18 and 60 years old who did not fit one or more of the exclusion criteria (chronic inflammatory or infectious diseases, pregnancy, and breastfeeding) were selected and had their blood collected by venipuncture. The infection by *Plasmodium vivax* was confirmed by qPCR. Briefly, DNA extraction was done using the QIAamp DNA Blood mini kit (QIAGEN). The individuals were treated with a combination of chloroquine and primaquine, according to the recommended schedule and doses of the Brazilian Ministry of Health. Forty-five days after the diagnosis, the same patients (who were now symptom-free) had their blood collected again to confirm by qPCR that they were no longer infected by *P. vivax*. All patients were informed about the procedures and objectives of the study and agreed to participate by written consent.

Human peripheral blood mononuclear cells (PBMCs) were isolated using Ficoll-Paque reagent (GE Healthcare) according to the manufacturer's protocol. Then, the PBMCs were enriched for monocytes using immunomagnetic separation. Briefly, PBMCs were incubated with magnetic CD14 microbeads for 15 min and then loaded in an LS MACS® column which was placed in a magnet (MACS® separator). The cells were washed 3 times with PBS (pH 7.2) containing 0.5% bovine serum albumin (BSA) and 2 mM EDTA. Then, the column was removed from the separator and the CD14+ cells magnetically retained on the column were eluted. The microbeads, columns, and magnets were all purchased from Miltenyi Biotec.

Total mRNA from the monocytes was extracted using TRIzol reagent (Thermo Fisher Scientific), quantified in a fluorometer (Qubit 2.0®, Thermo Fisher Scientific), and analyzed by capillary electrophoresis (Bioanalyzer®, Agilent) to certify its quality. Libraries were prepared from the mRNAs using the TruSeq Stranded mRNA Kit (Illumina) according to the manufacturer's protocol. The sequencing reaction was performed in a NextSeq 500 system using the NextSeq 500/550 High Output Kit v2.5 for 75 cycles (both from Illumina). The sequencing FASTQ files were processed with the Trimmomatic software to exclude bases with quality scores below 25 and remove adaptor sequences and short reads (less than 55 bases). The processed reads were then aligned to *Homo sapiens* genome reference (release 38) using STAR. DESeq2 software was used to obtain differentially expressed genes by a paired analysis in the contrast between the monocytes collected in the acute phase of the disease and those collected post-treatment for the same patients.

Public metabolomics and transcriptomics analyses

Normalized liquid chromatography-mass spectrometry (LC-MS) metabolomics data from the plasma of C57BL/6 mice infected with *Pc* were retrieved from the Metabolomics Workbench database under accession ID ST001775. Metabolomics data from the plasma of human volunteers experimentally infected with *P. vivax* were acquired from the MetaboLights repository under accession ID MTBLS665. The pre-processed feature table of negative mode LC-MS was log₂ transformed before statistical analysis and identification of itaconate was obtained via comparison of accurate mass (10 ppm) and retention time to that of the chemical reference standard. Transcriptomics data were acquired at the Gene Expression Omnibus (GEO) repository. We downloaded RNA sequencing (RNAseq) raw gene count tables of monocytes isolated from children, which were later stimulated with *P. falciparum*-infected red blood cells (iRBC) *in vitro* (GSE151116); of monocytes isolated from children during acute and convalescence phase of malaria caused by *P. falciparum* (GSE154317); and of effector memory CD4⁺ T cells sorted from adult volunteers experimentally infected

with *P. falciparum* before infection (baseline) and 6 days after drug treatment (GSE174791). Data were filtered, normalized to counts per million reads (CPM), and log-transformed using the EdgeR package for R. Statistical analyses of target metabolites or genes were performed with T-test or Mann–Whitney U test for categorical or Kruskal–Wallis test followed by Dunn’s multiple comparison test for longitudinal comparisons. Significance is given as * $p < 0.05$, ** $p < 0.01$, and *** $p < 0.001$.

Oxygen consumption rate and extracellular acidification in MODCs

After positive selection, CD11b⁺ splenocytes from infected and non-infected mice were plated on an xFe96 plate. The plates were previously coated with poly-D-lysine. The cells were incubated for 1 h with the appropriate treatment (UK5099, Etomoxir, DON, or GW9662). After the treatment, the media was changed, the treatment was replaced, and cells were incubated for 1 h in an incubator without carbon dioxide. After incubation, the cells were placed in the Seahorse XFe96 Analyzer for MitoStress Assay. During the assay, the first three quantification measures the basal oxygen consumption. Three quantifications were performed after each injection with Oligomycin 1.5 mM, FCCP 1.5 mM, and Rotenone/Antimycin 0.5 mM. The parameter of maximal respiration was obtained from the average quantification after FCCP treatment minus the average of measurements after Rotenone and Antimycin treatments. The basal levels of extracellular acidification were quantified before the injection with Oligomycin.

QUANTIFICATION AND STATISTICAL ANALYSIS

Results are presented as mean \pm SEM. All graphs were generated by GraphPad Prism 9.0 (GraphPad Software, La Jolla, CA, USA). The sample distribution was determined by a Kolmogorov–Smirnov normality test. For statistical comparisons, one-way ANOVA tests were used to compare normally distributed variables. Non-normally distributed data were compared using the Kruskal–Wallis test. The analysis of untargeted metabolomics, untargeted lipidomics, and transcriptomes is described in the subsection that respectively describes each omic data.